Micro-analytical Perspectives on the Bishop Tuff and its Magma Chamber

K. J. CHAMBERLAIN[1,2*], C. J. N. WILSON[1], P. J. WALLACE[3] AND M. -A. MILLET [1,2]

[1]SCHOOL OF GEOGRAPHY, ENVIRONMENT AND EARTH SCIENCES, VICTORIA UNIVERSITY, PO BOX 600, WELLINGTON 6140, NEW ZEALAND

[2] DEPARTMENT OF EARTH SCIENCES, UNIVERSITY OF DURHAM, DURHAM DH1 3LE, UK

[3] DEPARTMENT OF GEOLOGICAL SCIENCES, UNIVERSITY OF OREGON, EUGENE, OREGON 97403-1272, USA

This is a pre-copyedited, author-produced version of an article accepted for publication in Journal of Petrology following peer review. The version of record is available online at: https://doi.org/10.1093/petrology/egv012

Manuscript for: *Journal of Petrology*

Running title: Micro-analytical perspectives on the Bishop Tuff

Keywords: Bishop Tuff, supereruption, magma chamber, compositional zoning, magma mixing.

Final accepted version

*Corresponding author. Phone (+44) 191 334 2300, Fax (+44) 191 334 2301
Email addresses: katy.chamberlain@dur.ac.uk; colin.wilson@vuw.ac.nz; pwallace@uoregon.edu; m.a.millet@durham.ac.uk

ABSTRACT

New in-situ major and trace element analytical data from crystals (sanidine, plagioclase, biotite, orthopyroxene, clinopyroxene) and matrix glasses are presented from juvenile materials representing the full Bishop Tuff sequence from the earliest fall unit (F1) to the latest ignimbrite package (Ig2Nc). These data are combined with published information to investigate the nature and zonation of the pre-eruptive Bishop magma chamber. Our data confirm that this magma chamber was a single unitary body which was thermally and compositionally zoned. The zonation was largely established prior to the growth of crystals, and also prior to mixing in the lower parts of the chamber induced by late-stage intrusion of a magma of contrasting composition and slightly hotter temperature (the 'bright-rim' magma). Sparse mixed swirly and dacitic pumices show enrichments in Ba, Sr and Ti that identify these pumices as possible representatives of the 'bright-rim' magma. A model (revised from previously published work) for the pre-eruptive magma chamber comprises three main parts: (i) an upper, volumetrically dominant (~2/3), relatively unzoned region which was the source of the earlier, eastern-erupted ignimbrite units and their coeval fall units; (ii) a volumetrically minor transition zone which shows evidence for minor degrees of mixing and was the dominant source for the latest, eastern-erupted part of Ig1Eb (Sherwin subunit) and the earlier part of the northern-erupted ignimbrite (Ig 2Na); and (iii) a lower, volumetrically subordinate (~1/3) region which was affected by mixing with the 'bright-rim' invasive magma in the lead-up to the eruption, and fed later northern-erupted units. Ingress of the 'bright-rim' magma introduced orthopyroxene and bright-rimmed zircon crystals, induced partial resorption then overgrowth of rims enriched in Ti, Sr and Ba on sanidine and quartz, and development of zoning in clinopyroxene. Based on pumice proportions and associated crystal and glass chemistries through the eruptive sequence, we infer that the roof and floor of the magma chamber were stepped down to the north, such that the transition

zone magma formed the floor of the southern part of the melt-dominant chamber and the roof of the northern part. Our data reinforce the previous concept of a single compositionally and thermally zoned Bishop magma chamber and additionally provides a temporally constrained role for pre-eruptive magma mixing and the introduction of melts and minerals with contrasting compositions to the resident Bishop magma.

INTRODUCTION

Supereruptions (those involving >10^{15} kg or ~450 km^3 of magma: Sparks *et al.*, 2005; Self, 2006; Miller & Wark, 2008) are the largest explosive volcanic eruptions on Earth, with both devastating immediate impacts and significant long-term environmental consequences (e.g. Rampino & Self, 1993; Sparks *et al.*, 2005; Self, 2006; Self & Blake, 2008). Because of the comparative scarcity of these events, it is necessary to examine the geological record in order to understand the processes by which these giant magma bodies are assembled and stored in the crust, and how their eruptions are triggered.

The Bishop Tuff is an iconic example of a supereruption deposit formed from the eruption of >600 km^3 of compositionally- and thermally-zoned silicic magma (Hildreth & Wilson, 2007), and has been a focal point for >35 years of reconstructions of large magma chambers. The wealth of analytical investigation that has been undertaken on the Bishop Tuff (including, but not limited to: Hildreth, 1977, 1979; Halliday *et* al., 1984; Dunbar & Hervig, 1992a; Hervig & Dunbar, 1992; Christensen & DePaolo, 1993; Christensen & Halliday, 1996; Davies & Halliday 1998; Wallace *et al*., 1999; Anderson *et al*., 2000; Reid & Coath, 2000; Bindeman & Valley, 2002; Simon & Reid, 2005; Hildreth & Wilson, 2007; Simon *et al*., 2007; Wark *et al*., 2007; Reid *et al*., 2011; Gualda *et al*., 2012a; Pamukcu *et al*., 2012; Roberge *et al*., 2013; Chamberlain *et al*., 2014a; Simon *et al*., 2014) has led to it being used as a case study to build and refine models applied to the origins of large-volume, high-silica

rhyolitic volcanism. These models not only include those used to investigate the generation and evacuation of these supereruptive units (including the magma 'mush model'; e.g. Bachmann & Bergantz, 2004; Gualda *et al*., 2012a; Carrichi *et al*., 2014; Malfait *et al*., 2014) but also the calibration of geothermometers such as Ti-in-quartz and Fe–Ti-oxide (e.g. Wark *et al*., 2007; Thomas *et al*., 2010; Thomas & Watson, 2012; Wilson *et al*., 2012; Evans & Bachmann, 2013; Ghiorso & Gualda, 2013; Evans *et al*., 2015).

Although extensively studied, there is currently debate around the Bishop magma system, centred around the mineral (rather than glass and melt inclusion) records, with two contrasting approaches and conclusions.

(1). As originally proposed by Hildreth (1977, 1979), the Bishop Tuff was erupted from a unitary body of magma that was compositionally- and thermally-zoned prior to crystal growth. This hypothesis was established using comprehensive petrography and analysis of all crystal phases in the Bishop Tuff. The variations in crystal composition (interpreted to reflect growth of crystals in the melt in which they were found) thus were taken to reflect compositional stratification of the Bishop magma chamber, prior to crystallisation, from upper, more-evolved, cooler to lower, less-evolved, hotter magma (Hildreth, 1977, 1979; Hildreth & Wilson, 2007). This hypothesis has been strengthened by further whole-rock data (e.g. Hildreth & Wilson, 2007), and melt inclusion studies which show that the upper-regions of the magma chamber were richer in water, and poorer in CO_2 when compared with the lower, less-evolved, water-poorer, CO_2-richer regions of the Bishop magma chamber (Dunbar & Hervig, 1992a; Wallace *et al*., 1995, 1999; Anderson *et al*., 2000; Roberge *et al*., 2013). This compositional gradient is mirrored by an inferred thermal gradient of 80-100 °C, with coolest temperatures (modelled from Fe-Ti oxide, $\delta^{18}O$ (Qtz-mt), and two-feldspar thermometry: Hildreth 1977, 1979; Bindeman & Valley, 2002; Hildreth & Wilson, 2007; Ghiorso & Evans, 2008; Chamberlain *et al*., 2014b) being at the top of the magma chamber.

(2). Building on suggestions that either or both of the Fe-Ti oxides and pyroxenes are not in equilibrium with the melt (Andersen & Lindsley, 1988; Lindsley *et al*., 1991), thermodynamic modelling has been used to suggest that values for pre-eruptive temperature gradients are flawed (Ghiorso & Gualda, 2013). Associated Rhyolite-MELTS modelling and silica-in-glass barometry of the Bishop Tuff has been used to assert that there was no significant thermal or pressure gradient within the Bishop magma chamber, with all samples [from the Hildreth (1977) dataset] displaying apparent pressures and temperatures of 175 – 200 MPa and 740 – 750º C, respectively (Gualda *et al*., 2012a; Gualda & Ghiorso 2013a,b). This similarity of pressure and temperature estimates combined with a perceived bimodality of crystal compositions, has led to the hypothesis that the Bishop Tuff is the product of the eruption of two chemically distinct and physically separated magma bodies (Gualda & Ghiorso, 2013a), with analogues drawn from the multiple magma bodies of the Kidnappers (Cooper *et al*., 2012) and Mamaku/Ohakuri (Gravley *et al*., 2007) eruptions in New Zealand.

The dependence of many models for silicic magmatism on data and concepts from the Bishop Tuff means that developing an accurate understanding of the nature and stratification (both thermal and compositional) of the pre-eruptive Bishop magma body is of great importance. Debates regarding the nature of the Bishop Tuff magma body (or bodies) have, however, relied solely on the original compositional data for pumices and crystals (as compared to melt inclusions) of Hildreth (1977, 1979)(e.g. Evans & Bachmann, 2013; Gualda & Ghiorso, 2013a). Only Fe–Ti-oxide compositional analyses and bulk rock analyses have been carried out since (Hildreth & Wilson, 2007). In order to properly address the issues raised above, we present detailed *in-situ* analyses of crystals and glasses from the Bishop Tuff, that integrate textural and trace element compositional variations at the scale of tens of microns. We combine our spatially-resolved crystal compositional data with the eruptive stratigraphy of Wilson & Hildreth (1997) and Hildreth & Wilson (2007) to:

(a) re-address the composition of and stratification within the Bishop Tuff magma body,

(b) decipher the nature and role of the contrasting magma which gave rise to compositionally contrasting rims on sanidine, quartz and zircon (Wark *et al*., 2007; Gualda *et al*., 2012b; Chamberlain *et al*., 2014a,b), and

(c) investigate the role of subordinate, poorly preserved ignimbrite packages (Ig1SW, Ig1NW, Ig2SW; Fig. 2) in constraining any variability in the Bishop magma chamber.

THE BISHOP TUFF

The Bishop Tuff was erupted at 767.4 ± 2.2 ka (Rivera *et al*., 2011), accompanying the formation of Long Valley caldera in eastern California (Fig. 1: Bailey *et al*., 1976; Hildreth, 1979, 2004; Bailey, 1989; Wilson & Hildreth, 1997; Hildreth & Wilson, 2007). The >600 km^3 of high-silica rhyolite magma is inferred to have been erupted, with possibly one short hiatus, over a period of ~6 days (Wilson & Hildreth, 1997). The Bishop Tuff represents the culmination of 4.5 Myr of magmatism in general and >1.4 Myr of rhyolitic volcanism in particular in the Long Valley region (Bailey *et al*., 1976; Metz & Mahood, 1985, 1991; Metz & Bailey, 1993; Bailey, 2004; Hildreth, 2004; Sarna-Wojcicki *et al*., 2005). In its proximal outcrop area between the Sierra Nevada and the White Mountains (Fig. 1) the tuff consists of nine fall units (F1-F9, Fig. 2), now preserved within a 90° sector east of the caldera, and multiple largely coeval ignimbrite packages (Ig1Ea to Ig2Nc: Fig. 2) mostly deposited in two sectors to the north and east of the caldera margin (Fig. 1). Lithic assemblages in the tuff link earlier erupted units to a vent area sited in the south-eastern part of what became the caldera, and reflect in their changes the subsequent concurrent development of venting along the northern and eastern portions of the caldera ring fracture (Figs. 1, 2: Hildreth & Mahood, 1986; Wilson & Hildreth, 1997).

Through the Bishop Tuff, the types and proportions of pumice change systematically (Hildreth & Wilson, 2007), in general from the dominance of crystal-poor (xp; <6 wt%) pumice in the earlier erupted units (F1-F8; Ig1 packages deposited mostly east of source) through crystal-moderate (xm; 6-12 wt %) to crystal-rich (xr; >12 wt %) pumice in the later erupted ignimbrite, deposited mostly north of the contemporaneous caldera rim. Petrographic studies (Hildreth, 1977, 1979) showed that sanidine and quartz are the most common crystal species present in the Bishop Tuff, found in roughly equal proportions. Plagioclase crystals commonly make up ~10% of the crystal assemblage. When combined, sanidine, quartz and plagioclase make up 98 – 99% of the total crystal population of the Bishop Tuff. Minor proportions of titanomagnetite and biotite are ubiquitous throughout the Bishop Tuff. Even less abundant, but present throughout the stratigraphy are ilmenite, zircon and apatite. Allanite is present in only earlier-erupted Bishop Tuff, while in contrast clinopyroxene and orthopyroxene are only present in later-erupted Bishop Tuff: Ig2E and all northern-erupted units (Hildreth & Wilson, 2007).

Studies of volatiles in quartz-hosted melt inclusions show a general decrease in water and increase in CO_2 contents and inferred melt inclusion entrapment pressures from earlier, eastern eruptives into later, northern units (Dunbar & Hervig, 1992a; Wallace *et al*., 1999; Anderson *et al*., 2000; Roberge *et al*., 2013). The earlier eastern deposited ignimbrite units, together with their coeval fall deposits, are consequently inferred to represent the upper part of the magma body (depths as shallow as 5-6 km), whereas the later, northern-deposited ignimbrite packages are thought to represent magma erupted from deeper (up to 10-11 km) in the magma chamber (Wallace *et al*., 1999).

Prior to eruption of the Bishop Tuff the rhyolitic Glass Mountain system was in operation from ~2.2 Ma (and possibly earlier: Chamberlain *et al*., 2014a) to ~860 ka producing more than 60 effusive and explosive eruptions (Metz & Mahood, 1985, 1991;

Halliday *et al*., 1989; Metz & Bailey, 1993; Hildreth, 2004; Chamberlain *et al*., 2014a; Simon *et al*., 2014). These eruptions built an edifice of domes and associated pyroclastic fans which were partly truncated by the Bishop caldera collapse, but the remaining part of which served to provide a topographic high which divided the northerly and easterly-directed Bishop pyroclastic flows. Recent eruption age estimates [by U-Pb determinations on zircon (Chamberlain *et al*., 2014a) and $^{40}Ar/^{39}Ar$ age experiments (Simon *et al*., 2014)] both indicate that eruption of the youngest Glass Mountain dome occurred ~95 kyr prior to the climactic Bishop Tuff eruption.

SAMPLING AND ANALYTICAL TECHNIQUES

Sixty samples of the Bishop Tuff were analysed (Table 1), selected to represent all ignimbrite packages, plus fall units 1, 2, 7 and 9 (Fig. 2). Pumice clasts were chosen to span the range of 'normal' crystal-poor (xp) to crystal-rich (xr) clasts, as well as the 'variant' pumice types, including those labelled as chocolate (dark), swirly, and dacitic, as defined by Hildreth & Wilson (2007). For a full description of pumice textures in the Bishop Tuff see Hildreth & Wilson (2007). Where possible, single pumice clasts were used; however, if this was not feasible, multiple lapilli-sized pumice clasts were collected. All clasts were cleaned of any adhering matrix prior to sample preparation. Full details of all samples collected and analyses undertaken are in Table 1.

Pumice clasts were rough crushed using a Boyd crusher, and sieved to various size fractions. Crystals were hand-picked from the 1-2 mm (feldspars), 0.5-1 mm (biotite, glass) or 250-500 μm (pyroxenes) sieve fractions, mounted into epoxy discs, polished to expose the crystal cores and carbon coated for imaging and analysis. Although pyroxenes, both ortho- and clino-, have been reported from the later-erupted northern material, and some Sherwin subunit (latest Ig1Eb) and later eastern (Ig2Eb,c) pumices (Hildreth, 1977, 1979; Hildreth &

Wilson, 2007), pyroxenes were only recovered from the Ig2NWa, Ig2NWb, Ig2Nb and Ig2Nc samples in this study, with no appropriately sized (≥250 μm) pyroxenes present in any other samples. Major element analyses were obtained on a JEOL JXA 8230 electron probe microanalyser (EPMA) at Victoria University of Wellington (VUW) using wavelength-dispersive spectrometry. Prior to analysis, back-scattered electron (BSE) images were taken of all crystal phases to identify zoning patterns and locate the analytical spots. Precision of standard analyses of major elements (>5 wt.% concentration) is nearly always within 5 relative % (2 s.d.); uncertainties are slightly higher for minor elements (for details see Electronic Appendix 1). For biotite, non-stoichiometric analyses with totals of <95 wt.% and anomalous K_2O concentrations were set aside (as per Hildreth, 1977). Similarly, glass analyses with totals of <93 wt.% were set aside; values for the remaining analyses were then normalised to 100 %.

Trace element analyses were measured *in situ* using a New Wave deep UV laser (193 nm solid state) coupled to an Agilent 7500cs inductively coupled plasma mass spectrometer (ICPMS) at Victoria University of Wellington (VUW). The laser ablation (LA)-ICPMS data were internally normalized to ^{29}Si or ^{43}Ca from EPMA analyses. Abundances of single trace elements were calculated relative to a bracketing standard (NIST 612 or BCR-2G) which was analysed throughout the run under identical conditions. Precision and accuracies varied depending on the analytical conditions but generally have <5% (2 s.d.) uncertainties on elements with abundances of >20 ppm (slightly higher for less abundant elements: for details see Electronic Appendix 1).

RESULTS

Sanidine

Sanidine is one of the two most abundant crystal species in the Bishop Tuff, making up ~40% of the crystal population (Hildreth, 1977, 1979; Hildreth & Wilson, 2007). Sanidine crystals from eastern units are dominantly unzoned under BSE (Fig. 3) reflecting the lack of compositional variation measured by EPMA analyses (Fig. 4). Of 28 samples from all eastern ignimbrite and most fall (F1-F8) units, only two (BP032 and BP244) contained sanidine grains with bright rims in BSE imagery (10 and 25% of the grains imaged, respectively: Table 1). The nine samples from F9, Ig2NWa and Ig2Na have 14 to 45% of their sanidine with bright rims, while the eleven late northern (Ig2NWb, Ig2Nb, and Ig2Nc) samples have 45% to 100 % of bright rimmed sanidine (Figs. 2 and 3; Table 1). Swirly or dacitic pumices additionally sometimes include anomalous sanidine grains which are commonly fractured, cloudy and completely bright under BSE, and are thus interpreted as xenocrystic (Fig. 3). These grains are not included in the percent bright rim figures listed in Table 1.

Major element (n = 1403) and trace element (n = 834) analyses of sanidine crystals show limited ranges in composition for most elements, with most variations being within the 2 s.d. analytical uncertainty (Table 2; Fig. 4a). 97% of sanidine compositions are Or_{60} to Or_{68} with variations outside this range found only in xenocrystic grains ($Or_{>68}$) or rare examples of other overgrowth rims ($Or_{<60}$), enriched in Na_2O, found only in samples from northern vented ignimbrite packages from the north side of the caldera.

In terms of major elements (i.e., those measured using EPMA), sanidine from eastern deposited units (both fall deposits and ignimbrite) has only low-Ba concentrations relative to northern deposited units even if bright rims are visible from BSE images and irrespective of whether cores or rims are analysed. Although commonly enriched overall in Ba (and also Ca) when compared with sanidine in eastern-deposited units, sanidine from the northern vented ignimbrite packages is much more variable in its zoning patterns. These patterns range from low-Ba cores and rims (43% of sanidine), to low-Ba cores and higher Ba rims (47%), to

moderate Ba cores, with higher Ba rims (10%). Sanidine cores in both eastern and northern units are always depleted in Ba relative to their rims. The differences, however, between cores and rims in eastern sanidines are always <3500 ppm Ba, whereas in northern sanidines the core-rim differences are larger, up to 11000 ppm Ba. When all the sanidine major element data are considered as a whole, two modes of composition can be identified using Ba contents (as in Gualda *et al*., 2012a; Fig. 4b), although it is apparent that these lower-Ba and higher-Ba modes are represented by core and rim analyses in northern sanidines, respectively, often within the same crystal (Fig. 3). Ig2Na sanidine shows the most evolved compositions of samples from northern ignimbrite units, with major element compositions which overlap most closely with sanidine from eastern ignimbrite units.

In terms of trace elements, increases in Ba, Sr, Ti, and the light Rare Earth Elements (LREE) are the most significant, especially in the bright rim overgrowths that are common in sanidine from the later-erupted northern units. Sanidine zones with higher-Ba (dominantly represented by rims in northern vented units) commonly also show enrichments in Mg, Sr and LREE and depletions in Rb (Table 2; Fig.4) relative to the lower-Ba group (typified by cores and rims in eastern vented samples, and cores in northern vented units).Within the lower-Ba grains from eastern ignimbrite units there are still slight rimwards increases in Ba, only resolvable by LA-ICPMS analysis, to maximum concentrations of ~800 ppm, even in grains where BSE-visible bright rims are absent and EPMA could not resolve any changes in Ba concentration. Sanidine from swirly and dacite pumices has trace element characteristics that are indistinguishable from each other, as well as from sanidines in 'normal' pumice samples (Fig. 4f). The xenocrystic sanidine grains (identified by BSE imagery), however, have much higher Ba, Sr and Ca concentrations.

Plagioclase

Plagioclase is the third most abundant mineral species in the Bishop Tuff, making up ~10% of the crystal population (Hildreth, 1977, 1979; Hildreth & Wilson, 2007). Two groups of plagioclase have been identified using BSE imagery and confirmed with EPMA data. The first group is completely unzoned, whereas the second group shows faint oscillatory zoning (Fig. 3). These oscillatory-zoned crystals are generally only found in the late, northern vented samples, and there form 17 to 100% of the total plagioclase population per pumice sample.

Major- (n = 251) and trace-element (n = 310) analyses were carried out on Bishop plagioclase (Tables 1 and 3). In tune with observations from BSE imagery, two plagioclase populations are identified based on CaO content, similar to those reported in Gualda *et al*. (2012b), yet the changes in CaO content recorded by us are continuous, rather than bimodal. A higher-Ca group of crystals (CaO >4.4 wt.%; $>An_{22}$) is dominated (82%) by the oscillatory-zoned plagioclase, whereas a lower-Ca group (CaO <4.4 wt.%; $<An_{22}$) are dominantly (>65%) unzoned in BSE imagery. Unlike in the sanidine, there are no systematic differences between cores and rims of plagioclase, with only ~5% of crystals showing an overgrowth of a lower- or higher-CaO rim over a higher/lower-CaO core (not shown). Similar to the sanidine, northern-sourced plagioclase represents almost the entire range in CaO content, with only a single eastern-sourced sample (BP198), which has visual evidence for magma mixing in hand sample, reaching the higher-Ca compositions common in northern samples. The lower-Ca plagioclase, present throughout all Bishop Tuff samples, has no identifiable differences in its composition between eastern vented (earlier-erupted) versus northern vented (later-erupted) samples. The higher-Ca plagioclase has corresponding enrichments in Sr, Ba, Ti (Fig. 5) as well as Mg, Eu and LREE when compared with the lower-Ca plagioclase. The lower-Ca plagioclase shows weak positive correlations between Sr and Ba, or LREE, which do not vary based on either stratigraphic position or core-to-rim variations, in contrast to the changes observed in sanidine.

313

314 **Biotite**

315 Biotite is the most common ferromagnesian phase in the Bishop Tuff, increasing in
316 abundance from <0.05 vol.% in early fall units to ~0.5 vol.% in late northern ignimbrite
317 (Hildreth, 1979). Biotite was extracted from 25 pumices from early fall units to late-erupted
318 ignimbrite (Table 1). Although commonly found as golden brown weathered crystals, every
319 effort to select the freshest looking black biotite was made. Where present, biotite occurs as
320 euhedral crystals which display no evidence for dissolution. When imaged under BSE, no
321 zoning was evident in any crystals. 236 usable major element compositions were determined
322 (where usable here refers to totals >95 wt.%) from fresh biotite crystals. Biotite from early-
323 erupted units (Ig1E, fall units 1-8) systematically produced low totals (Table 4) due to strong
324 interlayer deficiencies in K_2O, and so could not be used for accurate comparisons. This
325 alteration has been attributed to syn-eruptive destabilisation of biotite in the upper, more
326 water-rich parts of the Bishop magma chamber (Hildreth, 1977). Although limited by the
327 varying degrees of weathering which they have undergone, later-erupted biotite crystals are
328 enriched in TiO_2 and extend to lower K_2O values than earlier-erupted biotite. No other
329 differences in major element chemistry can be discerned from the EPMA data (Fig. 6).
330 Variable degrees of biotite alteration are noted in all samples (similar to Hildreth, 1977, 1979)
331 therefore further investigation using trace element analyses was not undertaken, and the value
332 of biotite in investigating or constraining the nature of the pre-eruptive magma body may be
333 limited.

334

335 **Orthopyroxene**

336 All orthopyroxene present is euhedral, and in BSE imagery shows no evidence for any late-
337 stage dissolution. Using high contrast BSE imagery, some zoning is discernible, with Mg#

values obtained from subsequent EPMA analyses varying from 48.2 to 56.3 (Fig. 7). Orthopyroxene displays a range in zoning textures which define four groups: 1) completely unzoned; 2) simple zoned with a BSE-brighter (Fe-richer) rim; 3) simple zoned with a BSE-darker (Mg-richer) rim; and 4) complexly zoned crystals (Fig. 3). The zoning style does not correlate systematically to any particular sample or eruptive unit (Electronic Appendix 2).

Major element analyses (n = 285) of orthopyroxenes show slight variations in SiO_2, MgO, FeO and CaO (Table 5; Fig. 7). Trace element analyses (n = 269) show that Mn and Zn are positively correlated (Fig. 7c), although no other trace elements show systematic variation (Fig. 7e). Interestingly, although slight zoning is evident under BSE imagery, there are no systematic major or trace element differences between cores and rims, even when only cores and rims from one zoning type is considered. Similarly, there are no systematic relationships in orthopyroxene composition with the crystallinity of the host pumice, its location in the eruptive stratigraphy or between different pumice textural groups (e.g. swirly vs. 'normal'; Fig. 7).

Clinopyroxene

Clinopyroxene occurs in similar proportions as orthopyroxene (Hildreth, 1977), and is only found in samples which also contain orthopyroxene. Similar to orthopyroxene, clinopyroxene is euhedral. Clinopyroxene BSE images commonly reveal more well-developed zoning patterns than in orthopyroxene, and again can be divided into 4 groups: unzoned crystals, those with a BSE-brighter rim, those with a BSE-darker rim and those with more complex zoning patterns (Fig. 3).

Major element analyses (n = 215) and trace element analyses (n = 143) of clinopyroxene were obtained. Clinopyroxene varies between 41.7% Wo and 44.2% Wo and major-element concentrations are relatively uniform with only slight variations in SiO_2, CaO,

MgO and FeO (Table 5; Fig. 7b). Trace elements are more variable than in orthopyroxene: Zn correlates negatively against Eu, Zr, Ni and Co, but correlates positively with Mn and Y, with no systematic variation in other trace elements. However, these observed variations do not correlate with core versus rims, pumice type (swirly vs. normal), crystal content, or by north versus northwestern ignimbrite packages (Fig. 7) where, similar to orthopyroxene, clinopyroxene cores and rims show the same ranges in trace element concentrations. Zoning type is also not a control on the observed trace element variations.

Glass host material

Fifty-six samples of separated glass fractions from the Bishop Tuff were analysed (Table 1). The data set comprises both major- (n = 1571) and trace-element (n = 697) analyses. Elements with concentrations close to their detection limits using EPMA were also analysed using LA-ICPMS techniques to improve precision and accuracy.

Glass chemistry from 'normal' early- and intermediate-erupted pumices

Pumices from F1-F8 and the eastern ignimbrite units (representative of earliest- to intermediate-erupted magma) with a range of crystallinity were analysed (see Table 1). Variations in major element glass chemistry are very restricted in eastern samples, all having SiO_2 contents (calculated volatile free) of 75.9-78.4 wt.% (±1.2 wt.%, 2 s.d. for SiO_2 analyses by EPMA; Table 6). Slight variations in K_2O, Al_2O_3, CaO and Na_2O are observed, but these are challenging to resolve beyond analytical uncertainty with EPMA techniques (Fig. 8). Trace element analyses of eastern glass reveal much more distinctive chemical variations and highlight systematic trends. The most evolved compositions, defined by those with the lowest Sr, Ba, LREE, Ca, Ti, Zr and Mg, and the highest incompatible element (Rb, Nb, Cs) contents (Hildreth, 1977, 1979) are found in the very earliest fall material (F1, F2) and some Ig1Ea

samples (Table 6; Fig. 8c). The measured variability within a single pumice increases with progression through the eruption, with some eastern samples displaying a twofold variation in Ba and Sr concentrations from different glass shards yielded by crushing of a single clast (Fig. 8c, d, f). By comparing the compositional data of eastern glass samples with data from glass matrices in pumices from the Ig1NW, Ig1SW and Ig2SW ignimbrite units, it is clear that samples from these units all share trace element characteristics similar to the 'normal' eastern type samples (Fig. 8), which includes some limited overlap with the 'normal' northern type samples.

Glass chemistry from 'normal' later-erupted pumices

Glass matrix samples from pumices in northern ignimbrite lobes (representative of later-erupted material) and unit F9 have more variable compositions than those from the earlier-erupted eastern samples, although SiO_2 values (75.4 to 78.3 wt.%, volatile free) cover a similar range. Glasses from northern samples are typically more enriched in Ba, Sr, LREE, Ti and Zr when compared with eastern glass, and similarly are more depleted in Mn, Rb, Nb, Cs, Th and U (Table 6; Fig. 8). Glass samples from Ig2Na and F9 have the most evolved compositions of all later-erupted material, apparently defining an overlap between earlier, more-evolved and later, less-evolved glass compositions (Fig. 8e). Single-pumice variations in glass compositions are also much greater in later erupted pumices than in earlier units, with Ba varying by up to ~100 ppm in glass within a single clast (Fig. 8c, d, f).

Glass chemistry from variant (swirly, dark) pumices

Of the clasts identified as 'swirly' or 'dark' (Table 1) only five showed any distinct differences from the suite of Bishop Tuff 'normal' pumice glasses. Samples BP032, BP197, BP198, BP230 and BP232 all show enrichments in Ca, Fe, Ti, Ba, V, Mn, Sr and Mg

compared with ‘normal’ Bishop glass (eastern and northern: Fig. 9a, b). There are, however, no variations in any REE, or Rb, Nb and Cs. Compositional variations within single clasts are very large within the swirly pumice suite, greatly exceeding those observed in any of the normal pumices.

Glass chemistry from dacitic juvenile clasts

Three less-evolved samples from Ig2NWb were examined, where black (or red, where oxidised) poorly vesicular material of dacitic composition is comingled with white rhyolite, (the dacites of Hildreth & Wilson, 2007). All three samples have dacite glass compositions which are distinctly different from all others measured in the Bishop Tuff. Instead of a continuum in glass chemistry, as evidenced from variable degrees of mixing in swirly samples, distinct bimodality is observed. The white rhyolite glass component of the dacitic clasts overlaps with the glass compositions of non-mixed pumices in the northern-vented Bishop ignimbrite. In contrast, the darker dacite (glass SiO_2 of 64.6 – 69.9 wt.%, volatile free) is significantly enriched (by up to 4 to 5 times: Table 6) in Ba, Sr, Mg, Ti, V, Ca, Zr, Eu and Ni, with accompanying depletions in Rb when compared with rhyolite glass (see Table 6; Fig. 9). This bimodality in glass compositions within single clasts shows that very little chemical mixing occurred between the rhyolite and dacite melts prior to or during eruption.

INSIGHTS INTO THE BISHOP MAGMA BODY

We use our major and trace element analyses of glass and phenocrysts from samples spanning the Bishop Tuff sequence to address four key issues about the Bishop magma system. In conjunction with our new data we utilise previously published data sets of major and trace element concentrations in melt inclusions (Dunbar & Hervig, 1992a; Wallace *et al*., 1999; Anderson *et al*., 2000; Roberge *et al*., 2013), zircon textures and trace element concentrations

(Reid *et al*., 2011; Chamberlain *et al*., 2014a) and quartz and sanidine zoning patterns (Anderson *et al*., 2000; Peppard *et al*., 2001; Wark *et al*., 2007; Chamberlain *et al*., 2014b). The issues we address are considered under headings as follows.

1). **Origins of Bishop crystals**. Did all the crystals grow in the melt/glass in which they are now found, as proposed by Hildreth (1977, 1979)? If not, then which crystals (or parts thereof) were sourced from what magmas?

2). **Compositional variations in the Bishop magma chamber.** What was the nature of the zonation within the pre-eruptive Bishop magma chamber, and what role did late-stage intrusion of the contrasting magma that gave rise to the CL-bright (zircon, quartz: Peppard *et al*., 2001; Wark *et al*., 2007; Chamberlain *et al*., 2014a) and BSE-bright (sanidine: Chamberlain *et al*., 2014b) rims have in establishing this zonation?

3). **Sources of subordinate ignimbrite packages.** Where in the magma body did the volumetrically subordinate or poorly preserved Ig1SW, Ig1NW and Ig2SW packages (Fig. 2; Wilson & Hildreth, 1997) originate? How do their compositional data relate to zoning within the Bishop magma chamber?

4). **Geometry of the Bishop magma chamber.** Is there geochemical evidence for a horizontal or stepped roof of the Bishop magma chamber, and how does our new data contribute to a revised magma chamber model?

In the sections below, we discuss the implications of our new data. In a subsequent section we address the current controversies about the Bishop magma system, including a proposal that the Bishop Tuff eruption was the product of two spatially distinct magma chambers.

Origins of Bishop crystals

We couple our new crystal and glass data with published information to consider the origins of the common Bishop Tuff crystal phases. Originally the hypothesis was advanced that all the crystals were phenocrysts that grew within the melt in which they were immersed on eruption (Hildreth, 1979) with no evidence of what would now be termed antecrystic major phases (e.g. Bacon & Lowenstern, 2005; Charlier *et al*., 2005, 2008; Miller *et al*., 2007; Allan *et al*., 2013). However, since Hildreth (1979) it has been recognised that many crystals in later-erupted units show a two-step history, precluding interpretation of all crystals as phenocrysts. The late-stage mixing event with the 'bright-rim' magma affected the deeper parts of the Bishop chamber, resulting in overgrowth of bright (under BSE or CL) crystal rims, richer in Ba and Sr in sanidine, richer in Ti in quartz, and poorer in U, Th and REE in zircon (Anderson *et al*., 2000; Peppard *et al*., 2001; Simon & Reid, 2005; Gualda, 2007; Hildreth & Wilson, 2007; Wark *et al*., 2007; Gualda *et al*., 2012b; Roberge *et al*., 2013; Chamberlain *et al*., 2014a,b).

Sanidine

Two-feldspar thermometry on plagioclase inclusions within sanidine cores, or sanidine inclusions within plagioclase cores, undertaken on the same samples used in this study, yields a range in model temperatures of ~80 °C (740 °C to 820 °C) from early eastern units to late northern units (Chamberlain *et al*., 2014b), similar to ranges in Fe-Ti oxide and O-isotopic model temperatures (see below and Bindeman & Valley, 2002; Hildreth & Wilson, 2007). When the previously published model temperatures are compared with our new trace element measurements in the host sanidine cores, those with higher temperatures also tend to have higher Ba, Sr and LREE concentrations (Fig. 10a). Similarly, the cores of all sanidine crystals from samples of later, northern units are enriched in Ba, Sr, LREE and Ti (Fig. 10c), highlighting their less-evolved nature when compared with sanidine cores from samples of

earlier eastern units. These variations and continuity of the data show that the sanidine crystals have been resident in the normal Bishop magma for their entire growth, consistent with melt inclusion compositions in quartz: when inclusions in CL-bright rims are excluded, there is a gradual change from more-evolved compositions in the earlier-erupted units, to less-evolved in the later-erupted samples (Roberge *et al*., 2013). It is important to note, however, that the cores of sanidine crystals grew in the less-evolved northern melt *prior* to mixing with the late-stage bright-rim magma, and thus could be considered antecrystic to the final erupted Bishop magma compositions- where only the rims are in equilibrium with the melt in which they were erupted (cf. Hildreth, 1979; Evans *et al*., 2015).

Plagioclase

Although there are no systematic differences in core compositions of lower-Ca plagioclase crystals from eastern and northern units of the Bishop Tuff (Fig. 10b), their euhedral appearance and the occurrence of plagioclase of similar composition as inclusions within sanidine indicates that the lower-Ca plagioclase crystals are phenocrysts. In comparison, the enrichments in Ti, Sr, Ba in higher-Ca plagioclase might be taken to suggest that this mode of plagioclase may not be phenocrystic, and may have grown either during or after late-stage intrusion of the 'bright rim' magma (e.g. Chamberlain et al., 2014b). To investigate this possibility we modelled the melt compositions from which the higher-Ca plagioclase crystallised, using the partition coefficients of Brophy *et al*. (2011). By comparing the modelled compositions to those measured in glasses from the rare dacite samples (as a proxy for the 'bright-rim' magma, see later discussion), we find that the modelled melt compositions cannot match the high Sr content of the dacite glasses (Fig. 11a). Furthermore, the plagioclase inclusions within the cores of non-BSE-bright sanidine crystals include some of higher-Ca composition. These pieces of evidence imply that the higher-Ca plagioclase

crystals, despite their slight compositional differences to the lower-Ca plagioclase, are not simply related to interactions with the 'bright-rim' magma, and are themselves also true phenocrysts. We infer that the overall spectrum of plagioclase compositions and generally (but not exactly) matching textures reflect subtle, second-order variations in volatile contents and melt compositions within the Bishop magma body.

Pyroxenes

Pyroxenes in the Bishop Tuff are suggested by some authors to be late-stage entrants into the magma chamber and not in equilibrium with the other mineral phases (Evans & Bachmann, 2013). Equilibrium between the Bishop pyroxenes (and between them and melt) is, however, suggested by their euhedral appearance (Fig. 3), by $\delta^{18}O$ values consistent with equilibrium between both pyroxenes and quartz, magnetite, zircon and titanomagnetite (Bindeman & Valley, 2002), and by the compositions of all crystal inclusions within pyroxenes being the same as those of glass-coated crystals (Hildreth, 1977; Hildreth & Wilson, 2007). Here we use our measured trace element concentrations in crystal cores from both ortho- and clinopyroxene [using the partition coefficients of Brophy *et al*. (2011) and Olin & Wolff (2010), respectively] to model melt compositions from which the crystals grew (Fig. 11). Clinopyroxene modelled-melt compositions overlap with the Bishop Tuff field, and are distinct from the fields of the dacite compositions (used as proxies for the 'bright-rim' magma; Fig. 11b), suggesting that the clinopyroxene is phenocrystic. In contrast, the orthopyroxene modelled-melt compositions, while partly overlapping the 'normal' Bishop field, also overlap with the measured dacitic glass (Fig. 11c) suggesting that at least some orthopyroxene is phenocrystic to the 'bright-rim' magma and was hence introduced into the pre-existing Bishop magma by magma mixing. Complexities in unravelling melt compositions from crystals arise from the assumption that the dacites represent the particular

melt from which the orthopyroxene crystallised. This may not in fact be the case: the 'bright-rim' magma may itself not be definable by one single melt composition, as suggested by the compositional heterogeneities in glasses from dacitic and swirly clasts. Although the two pyroxenes in the Bishop Tuff may have different origins, they are in apparent oxygen isotopic equilibrium (Bindeman & Valley, 2002), and lack evidence for wide-scale dissolution. We attribute this apparent equilibrium to the broadly similar pressures and temperatures of the two melts, and the lack of major compositional and thermal contrasts between the resident Bishop magma and the incoming 'bright-rim' magma.

Experimental studies yield contrasting perspectives on the origins of Bishop pyroxenes. Naney (1983) showed that at 200 MPa, high temperatures (~820 – 840 °C) and a water content of ~4.1 wt.% (these pressure and water content values being similar to those inferred from melt inclusions within late Bishop Tuff quartz: Wallace *et al*., 1999), both orthopyroxene and clinopyroxene would be stable. Conversely, at 200 MPa but with higher water contents and lower temperatures appropriate for modelling the early and middle Bishop Tuff (5.3 wt.% H_2O: Wallace *et al*., 1999; 711–758 °C: Chamberlain *et al*., 2014b), only clinopyroxene occurred. However melt inclusion entrapment pressures for the early and middle Bishop material are <200 MPa (Wallace *et al*., 1999), and the lower overall pressures for these materials could explain the absence of clinopyroxene. Scaillet & Hildreth (2001) reported that clinopyroxene (but not orthopyroxene) was stable at 200 MPa using starting composition of Ig2NWb rhyolite, and orthopyroxene (but not clinopyroxene) was stable in a dark variant pumice (67 wt.% SiO_2) from Ig1Eb in experiments run at similar P,T conditions to the rhyolites. Note, however, that Scaillet & Hildreth (2001) were unable to crystallise plagioclase or quartz at temperatures >710 °C in their experiments (cf. Naney, 1983).

In summary, our modelling of melt compositions from clino- and orthopyroxene cores is consistent or compatible with the experimental results to suggest that clinopyroxene was a

phenocryst phase in the deeper parts of the Bishop magma body. In contrast, we consider that orthopyroxene was stable in the 'bright-rim' magma, and only entered the Bishop magma chamber when mixing commenced. We would thus interpret the small and non-unidirectional zonation patterns seen in the ortho- and clinopyroxene crystals (Fig. 7) to reflect continued crystal growth in subtly contrasting domains of melt composition created during the mixing process.

Summary of crystal origins

Chamberlain *et al*. (2014a) suggested that zircons composed of 80-100% CL-bright material in pumices from late-erupted units of the Bishop Tuff grew largely or wholly within the 'bright-rim' magma (Fig. 12). In contrast, no sanidine or quartz crystals appear to have been phenocrysts resident in the 'bright-rim' melt with no purely BSE-bright sanidine found (apart from those with xenocrystic origins, identified by their anomalous appearance and compositions (Fig. 3a) and no purely CL-bright quartz observed (Chamberlain *et al.,* 2014b). This lack is inferred to reflect the slightly higher temperature of the 'bright rim' melt (Wark *et al*., 2007; Chamberlain *et al*., 2014a) and its less-evolved composition with lower H_2O and higher CO_2, which resulted in sanidine and quartz not being stable phases (cf. Naney, 1983). This inference is in turn consistent with the partial dissolution of cores observed in quartz and sanidine with bright overgrowths (Peppard *et al*., 2001; Wark *et al*., 2007; Gualda *et al*., 2012b; Chamberlain *et al*., 2014b). After interaction between the 'bright-rim' and pre-existing Bishop magmas, some cooling was required to allow resumption of quartz and sanidine crystallisation in the relevant part of the magma body with growth of bright rims from the mixed magma.

Our results and those of other workers cited above therefore suggest that sanidine, plagioclase and quartz are true phenocrysts to the original, zoned Bishop magma body that

was established prior to mixing with the 'bright rim' magma. Other accompanying phases in the early to middle-erupted parts of the Bishop Tuff (allanite, Fe-Ti oxides: Hildreth, 1979; zircons lacking bright rims: Chamberlain *et al*., 2014a) would similarly be inferred to be phenocrysts. This conclusion (matching that of Hildreth, 1979) is consistent with the interpretation that the Bishop magma body was assembled by piecemeal release of essentially aphyric (and compositionally slightly heterogeneous) melt batches from a common mush zone, which then rose to their respective levels of neutral buoyancy based on the slight compositional differences and underwent some crystallisation (Hildreth & Wilson, 2007). The clinopyroxene is phenocrystic to the deeper, hotter magma, but available evidence cannot discriminate whether this phase grew prior to introduction of the 'bright rim' magma, or was in part a product of mixing between the lower Bishop and 'bright-rim' magmas, or both (Fig. 12). Orthopyroxene and dominantly CL-bright zircon, in contrast, are inferred to be native only to the incoming 'bright-rim' magma (Fig. 11).

Compositional variations in the Bishop magma chamber

Vertical variations

As discussed in the previous section, use of two-feldspar thermometry (Chamberlain *et al*., 2014b) and trace element analyses within sanidine cores show a systematic change from more-evolved compositions, lower temperatures in the earlier eastern erupted units to less-evolved, compositions and higher temperatures in the later, northern erupted units of the Bishop Tuff (Fig. 10) *prior* to mixing with the 'bright-rim' magma. These variations in and continuity of the data show that the Bishop Tuff magma chamber was thermally and compositionally zoned before any late-stage mixing with the 'bright-rim' magma (Fig. 12)

To constrain the zonation within the magma chamber after mixing with the 'bright-rim' magma and immediately prior to eruption we use glass compositions from all units of

612 the Bishop Tuff. On the large scale, when considering only pumices which fall into the
613 'normal' xp to xr spectrum of Hildreth & Wilson (2007), a systematic progression is evident
614 in the glass trace-element data, from the most-evolved Ba, Sr, Ti-poor melt in the earliest fall
615 units, to less-evolved, Ba, Sr and Ti-enriched melt in the order of: early fall (F1- F6) – early
616 eastern ignimbrites (Ig1E) and F7 - F8 – late eastern units (Ig2E and Ig2SW) – Sherwin lobe
617 (geographically confined lobe of latest Ig1Eb) – Ig2Na (and F8/9) – Later northern units
618 (Ig2Nb/c; Ig2NW) (Table 6; Figs. 8, 13; Electronic Appendix 2). Although the Sherwin lobe
619 underlies Ig2E, in the geographically constrained segment of the chamber tapped by the
620 Sherwin lobe the melt was less-evolved than that sourcing Ig2E. The least-evolved glass
621 compositions (77.8 wt.% SiO_2; 0.50 wt.% CaO; 950 ppm Ti; 55 ppm Sr; 340 ppm Ba: Table
622 6) in normal pumices are found in Ig2Nb/c and Ig2NWa/b samples, with no systematic
623 difference between these units. However, given the mineralogical evidence for interaction
624 with the 'bright-rim' magma in these units, their glass compositions are interpreted to reflect
625 a mixture of the less-evolved Bishop and 'bright-rim' magmas (Fig. 12). The general
626 progression in glass compositions is in agreement with those reported from previous analyses
627 of matrix glass, melt inclusions, and whole rock samples (Hildreth, 1979; Lu *et al*., 1992;
628 Wallace *et al*., 1999; Anderson *et al*., 2000; Hildreth & Wilson, 2007; Roberge *et al*., 2013).
629 On a finer scale, we note that samples from Ig2Na (Figs. 6, 8, 11) share several
630 characteristics in common with samples from both northern (later) and eastern (earlier)
631 ignimbrites. Ig2Na glass chemistry overlaps both northern and eastern glass compositions
632 (Fig. 8e), with melt inclusions from this unit having Rb/Ce and Nb/Ce ratios that span almost
633 the entire range of matrix glasses from the Bishop Tuff (Roberge *et al*., 2013). Similarly to
634 eastern samples, plagioclase compositions are dominantly lower-Ca and pyroxene crystals do
635 not exceed 250 μm across, while the bright rims on sanidines and zircon crystals are less well
636 developed when compared with other northern samples (Table 1; Chamberlain *et al.*, 2014a,

their figure 4). This evidence points towards the intermediate nature of Ig2Na and serves to highlight the sequential nature of the mineralogical and geochemical changes from earlier, eastern-erupted, to later, northern-erupted units of the Bishop Tuff. Identification of the more limited role of the 'bright-rim' magma in Ig2Na pumices when compared with other northern-sourced ignimbrites, combined with restricted evidence for mixing preserved in melt inclusions from Ig2Ea/b (which varies with geographic location: Roberge *et al*., 2013), show the diffuse nature of the transition zone between the earlier- and later-erupted materials (Fig. 12). Thus, although evidence for significant mixing is restricted to the northern-erupted units, some indications of mixing are also present in later eastern-erupted units.

Lateral variations

Although the Bishop Tuff includes geographically confined ignimbrite packages, some with distinctive pumice suites (e.g. the Sherwin and Watterson subunits of Ig1Eb: Hildreth & Wilson, 2007), lateral variations within the Bishop magma body have not previously been investigated. By collecting samples from multiple locations within single defined units we here test what lateral variations existed (or were preserved during eruption) within the Bishop magma body (Table 1). In most units of the tuff, no identifiable lateral variability can be identified; for example, the Watterson subunit, distinguished from other Ig1Eb samples in the basis of its relatively high abundance of swirly pumices, is indistinguishable based on chemical composition (see Electronic Appendices 1, 2). Samples from the Sherwin subunit of Ig1Eb do, however, show some chemical differences from the rest of Ig1Eb. Glasses from the Sherwin subunit plot in comparable fields to those from Ig2E (Fig. 13), and extend the less-evolved compositions reached by eastern material (though not reaching the high Ba, Sr, LREE levels of northern material). Sample BP040 in the Sherwin subunit displays the common presence of thin CL-bright rims on zircons, in contrast to other Ig1Eb zircons where

such rims are absent (Chamberlain *et al*., 2014a). This subunit has also been noted to contain some pyroxene-bearing pumice (Hildreth, 1977). However, in all three samples from this unit no pyroxene >250 μm was recovered, similar to Ig2Na samples. The lack of zoned sanidine phenocrysts, or all-bright zircons in Sherwin subunit samples suggests that although some 'bright-rim' magma may have reached this sector or level within the magma chamber, it was not volumetrically significant (Fig. 12).

Some lateral variability is also evident in the northern ignimbrite, where packages Ig2NWa and Ig2Na were erupted largely coevally, albeit from different vents (Wilson & Hildreth, 1997). Samples from Ig2NWa are much more typical of the late northern units with prevalent zoning in sanidine, quartz and zircon, high proportions of high-Ca plagioclase, the presence of large (>250 μm) pyroxenes and the less-evolved nature of matrix glasses. We infer that the 'bright-rim' magma mixed more freely with the source regions of Ig2NWa than Ig2Na, even though melt inclusion data show broadly similar depths of origin for both of these units (Wallace *et al*., 1999; Anderson *et al*., 2000). These observations imply that some lateral heterogeneity was present that is interpreted to reflect uneven degrees of interaction of the 'bright-rim' magma within the main Bishop magma body (and variable development of the transition zone: Fig. 12).

Role and nature of the 'bright-rim' magma

Late-stage introduction of the 'bright-rim' magma affected the lower regions of the Bishop magma body (Hildreth & Wilson, 2007; Wark *et al*., 2007). Although the 'bright-rim' magma played a role in accentuating the vertical zonation in the chamber, it was not the sole or dominant cause for this zonation (cf. Dunbar & Hervig, 1992a; Bindeman & Valley, 2002), as indicated by the gradient in sanidine core compositions and two-feldspar model temperatures (Chamberlain et al., 2014*b*). Magma erupted from northern vents is thus a mixture of less-

687 evolved (evidenced by sanidine core compositions) Bishop rhyolite magma and, by
688 comparison, even less-evolved 'bright-rim' magma. Caldera-forming eruptions frequently
689 preserve evidence for immediately pre-eruptive introduction of less-evolved magmas which is
690 often cited as an eruptive trigger (e.g. Shane *et al*., 2005; Wilson *et al*., 2006; Wark *et al*.,
691 2007; Wilcock *et al*., 2013; Goff *et al*., 2014). However, in the case of the Bishop Tuff,
692 timescale estimates from diffusion studies (Chamberlain *et al*., 2014b) demonstrate that this
693 mixing with the major mineral phases occurred over a period of up to 500 years prior to
694 eruption and therefore cannot have been the immediate eruption trigger (cf. Wark *et al*.,
695 2007). Furthermore, age and textural evidence from zircons partially or wholly grown from
696 the 'bright-rim' magma suggest that interaction with deep roots of the Bishop system possibly
697 occurred up to 10 kyr before eruption (Chamberlain *et al*., 2014a).
698 The materials sampled in the Bishop Tuff that may most closely approach the end-
699 member contributor to the 'bright rim' magma are the rare, poorly vesicular dacitic juvenile
700 clasts found in unit Ig2NWb, intermixed with 'normal' Bishop rhyolite in hand sample. We
701 infer these dacites represent a very late-stage ingress into the lower parts of the Bishop
702 magma chamber due to the clear bimodality in glass chemistry within single samples (Fig. 9),
703 with no apparent exchange of any elements between the dacite and rhyolite portions of the
704 samples (in blue in Fig. 9). These dacites are the most primitive juvenile material found in the
705 Bishop ignimbrite with the least-evolved (BP211) having 65.65 wt.% SiO_2, 4.29 wt.% CaO,
706 3830 ppm Ti, 360 ppm Sr and 750 ppm Ba (Table 6). The dacites also plot as end-members
707 for the less-evolved (clearly mixed) swirly and dark pumices [such as the sample B443
708 investigated by Scaillet & Hildreth (2001): 67.26 wt.% SiO_2, 3.87 wt.% CaO, 460 ppm Sr and
709 1350 ppm Ba; Hildreth & Wilson (2007)] (Fig. 9) which are present in variable (but small)
710 proportions throughout the Bishop Tuff. Other dacite, swirly and dark pumices represent a
711 broad compositional continuum (Hildreth & Wilson, 2007; Fig. 9) from the least-evolved

712 dacite, suggesting that either: 1) varying degrees of mixing with the melts in the main Bishop
713 magma body occurred, or 2) sample variability reflects heterogeneity in the compositions of
714 late intruded magmas and hence that the 'bright-rim' magma cannot be defined by a single
715 composition. Given the extended time period over which interactions are inferred to have
716 occurred, both explanations seem plausible.

717 Wark *et al*. (2007) specifically hypothesised that a deep intruding CO_2-rich mafic
718 magma provided a heat source for dissolution of sanidine and zircon crystals (to supply Ba,
719 Sr and Zr) in an intermediate crystal cumulate (mush) zone between the melt-dominant
720 Bishop magma body and the intruded mafic magma. This melted material then itself was
721 intruded into the overlying magma body, triggered partial dissolution of quartz and feldspar
722 through higher temperatures and then initiated rim overgrowths on these crystals through
723 lowering of the water activity in the melt via CO_2 enrichment. This specific hypothesis,
724 however, is at odds with two lines of evidence. First, this process would not explain the
725 increased concentrations of both Ti and Zr in the dacites (see Electronic Appendix 2).
726 Second, the cores of CL-bright rimmed zircons in the Bishop Tuff samples are invariably
727 euhedral, implying that at no stage did the 'bright-rim' melts reach temperatures or
728 compositions sufficient to cause zircon dissolution.

729 The presence of pre-and post-caldera dacites of similar compositions to those erupted
730 with the Bishop Tuff (Bailey, 1989; Hildreth, 2004) imply that the 'bright-rim' magma is not
731 unique to the Bishop Tuff, and in fact may represent a more long-lived but sparsely erupted
732 magma type in the Long Valley region. Identification of CL-bright rims on some zircons
733 from dome OD of Glass Mountain (Chamberlain *et al*., 2014a) suggest also that ancestral
734 'bright-rim' magmas interacted with the Glass Mountain magmatic system. It is therefore
735 plausible that dacite was always present as part of the fractionating sequence of magmas
736 present during rhyolitic activity, but that it could not be erupted through the density trap in

737 the upper mush zones of the Glass Mountain and Bishop Tuff systems (cf. Hildreth, 2004, his
738 figure 7). Instead it was only able to be erupted at the surface, or mixed with an existing
739 rhyolitic magma chamber, when some other control, possibly tectonic, permitted its passage
740 through the density trap.
741
742 **Sources of subordinate ignimbrite packages**
743 Three less voluminous (or less well preserved) ignimbrite packages occur: Ig1NW, Ig1SW
744 and Ig2SW (Fig. 2). Given their geographically limited extent these units are often
745 overlooked, but could still yield important insights into the finer stratification of the Bishop
746 magma chamber. By combining our new crystal and glass data with previous field
747 observations, Ig1SW and Ig1NW are linked to a similar magma source as Ig1Eb (Figs. 4, 8;
748 Wilson & Hildreth, 1997; Hildreth & Wilson, 2007). This inference is supported also by the
749 similarity of Fe–Ti-oxide model temperatures and Rb/Sr systematics between these three
750 units (Hildreth, 1979; Christensen & DePaolo, 1993; Hildreth & Wilson, 2007). Ig2SW was
751 originally interpreted to originate from a similar source region to Ig1SW, but from a magma
752 that had slightly higher Fe–Ti-oxide temperatures, zircons with bright overgrowth rims (on
753 57% of all zircons) and minor pyroxene, indicating similar magmatic conditions to the
754 pumices examined from Ig2E (Hildreth, 1979; Hildreth & Wilson, 2007; Chamberlain *et al*.,
755 2014a). Our new glass and crystal compositional data confirm this interpretation. The
756 reported presence of minor pyroxene (Hildreth, 1979) and bright rims on zircons
757 (Chamberlain *et al*., 2014a) raises the possibility that Ig2SW tapped a magma similar to that
758 of the Sherwin subunit, which may thus have extended to around the SW quadrant of the
759 Long Valley caldera.
760
761 **Geometry of the Bishop magma chamber**

762 Here we collate our new results and previously published material to propose a revised model
763 (Fig. 14) for the pre-eruptive Bishop magma body. Our sanidine data highlight that this body
764 was zoned in temperature (Chamberlain *et al*., 2014b) and composition, prior to growth of
765 any crystal phases or any interaction with the 'bright-rim' magma, as previously proposed by
766 others (Hildreth, 1977, 1979; Wallace *et al*., 1999; Anderson *et al*., 2000; Hildreth & Wilson,
767 2007). We use the melt inclusion compositional data and entrapment pressure estimates of
768 Wallace *et al*. (1999), Anderson *et al*. (2000) and Roberge *et al.* (2013) to constrain the
769 depths of the magma body. It is established that the earlier-erupted units were largely, but not
770 entirely, sourced from vents along the southern and southeastern sides of the caldera ring
771 fracture (F1-F9 Ig1E; Ig2E; Ig1SW; Ig2SW; Ig1NW) and are volumetrically dominant
772 (roughly two-thirds) when compared with the later-erupted northern units (Hildreth &
773 Wilson, 2007). Our model is similar in many respects to that previously proposed, but
774 incorporates the following key aspects:
775 1) An asymmetric roof between the southern/eastern and northern vents, following
776 after and scaled from the model of Wallace *et al*. (1999). Crystal-poor (xp) pumice is rare
777 (<20 %: Hildreth & Wilson, 2007) in northern-erupted units. An important question in
778 constraining the shape of the chamber roof (cf. Fig. 13 of Wallace *et al*., 1999 versus Fig. 18
779 of Hildreth & Wilson, 2007), is whether this paucity of xp material represents a pre-eruptive
780 lack of xp, 'eastern-type' magma under the northern vents, or if the xp material had originally
781 been present but was drained laterally and erupted from the earlier vents (Hildreth & Wilson,
782 2007). We thus measured glass compositions from xp pumices from the northern ignimbrite,
783 to determine if any had 'eastern'-type glass chemistry, or were more evolved than glasses in
784 the co-erupted xr pumices. The data show (Fig. 15) that xp pumices in the northern ignimbrite
785 lobes have similar (or less-evolved) glass (and sanidine) compositions to the xr pumices
786 (similar to those of northern units, Fig. 8), with no clear correlation between crystallinity and

787 the compositions of matrix glasses or crystal textures (Table 1; Fig. 15). The xp pumices in
788 northern units thus simply reflect a lack of crystallisation or some degree of crystal-liquid
789 separation from the xr magma. These results imply that the 'eastern-type' magma was never
790 resident in any significant quantity under the northern vents, with the most-evolved magma
791 being that of the transitional zone, represented by Ig2Na (cf. Hildreth & Wilson, 2007), and
792 are consistent with a stepped upper roof to the magma chamber. Roberge *et al*. (2013)
793 reported xp pumices from Ig2NWa with quartz-hosted melt inclusions with evolved
794 compositions similar to those in the early erupted materials, but concluded that the host
795 pumices were accidentally incorporated, and not derived from magma underneath the
796 northern rim of the caldera.
797 2) A transitional zone highlighting the compositional continuum between upper and
798 lower regions of the single magma chamber (cf. Gualda & Ghiorso, 2013a: see later
799 discussion). This transitional region is represented by material forming Ig2Na (and to a lesser
800 degree the Sherwin unit of Ig1Eb), and covers the change from the eastern, more-evolved,
801 dominantly crystal-poor material, with unzoned phenocrysts and no pyroxene, to the northern,
802 less-evolved, dominantly crystal-rich material, with zoned phenocrysts and pyroxenes. The
803 transition zone (Fig. 14) is represented by magma that has sparse, thin CL- or BSE-bright
804 rims on sanidine, quartz and zircon and thus is interpreted to have had shortly pre-eruptive
805 interaction with material that had experienced some mixing with the 'bright-rim' magma. The
806 presence of such a transition zone is also consistent with the melt inclusion compositional
807 data of Roberge *et al*. (2013).
808 3) A stepped lower margin to the Bishop melt-dominant volume tapped during the
809 eruption (Fig. 14). The physically and compositionally distinctive 'Adobe-type' (Hildreth &
810 Wilson, 2007) xr pumices are rare in the eastern units, and therefore it seems improbable that
811 the corresponding less-evolved magma ever underlay the southern and eastern sectors of the

caldera in significant quantities. Crystal-rich pumices investigated from eastern-deposited units (with the exception of those from the Sherwin subunit) all have more-evolved, restricted glass and crystal compositions when compared with northern deposited samples (see Electronic Appendices 1, 2).

4) Diverse intrusions of the compositionally heterogeneous 'bright-rim' magma. The less evolved compositions represented by the rare mixed dacitic pumices from Ig2NWb (themselves a possible proxy for the 'bright-rim' magma) are inferred to have been fed from depth under the northern roots to the magma body. The 'bright-rim' magma itself likely represents multiple injections of compositionally heterogeneous magma over an extended time period, based on the diversity in glass compositions (Fig. 9) and the varied timescales for interaction with the main Bishop magma body (Chamberlain *et al*., 2014a,b). Variations in composition of the 'bright-rim' magma are schematically represented in Fig. 14 by various stalling levels within the underlying mush pile. Any diversity in the range of crystallisation and mush mixing/assimilation would produce slightly different compositions of the resulting magma that eventually reached levels where it mixed in with the overlying Bishop magma body or was captured as ejecta in the eruption.

CONTROVERSIES IN THE BISHOP TUFF

There are two areas of current controversy in and around interpretations of the record preserved in the Bishop Tuff. The first concerns the Fe-Ti oxides, whether or not they are in equilibrium with each other or the host melt and the validity of the model temperature estimates derived from co-existing magnetite-ilmenite pairs. The second concerns the vertical dimensions of the Bishop magma chamber, and whether it was one unitary body, or two separate bodies.

Fe–Ti-oxides – equilibrium or disequilibrium?

A major question regarding the origins of crystals in the Bishop Tuff has been the relationship between the pyroxenes, Fe–Ti-oxides and the surrounding melt (e.g. Hildreth, 1977, 1979; Lindsley *et al*., 1990, 1991; Frost & Lindsley, 1992; Hildreth & Wilson, 2007; Evans & Bachman, 2013; Ghiorso & Gualda, 2013). As discussed above, we conclude that the pyroxenes are phenocrystic to certain portions of the Bishop magma body. Here we consider the disputes around the validity of the record in Fe-Ti oxides (Ghiorso & Gualda, 2013; Evans & Bachmann, 2013; Evans *et al*., 2014) and consequent inferences about the thermal structure of the pre-eruptive Bishop magma body.

Analysis of coexisting Fe–Ti-oxide pairs using the Andersen & Lindsley (1988) calibration showed a range in model temperatures from 703 °C in early fall units, to 816 °C in late-erupted ignimbrite samples (Hildreth & Wilson, 2007). Closely similar model temperatures were reported by Ghiorso & Evans (2008) using their modified calibration and these results are reiterated by Evans & Bachmann (2013) and Evans *et al*. (2014). The general values and ~100 °C range in Fe–Ti-oxide model temperatures from bottom to top of the Bishop Tuff are consistent with those derived from $\delta^{18}O$ thermometry utilising the fractionation of ^{18}O between quartz and magnetite (715 °C – 815 °C; Bindeman & Valley, 2002). Applications of Ti-in-quartz and Ti-in-zircon thermometry also yielded a ~100 °C temperature gradient (Wark *et al*., 2007; Reid *et al*., 2011) but the veracity of these model values is challenged by the assumptions associated with the appropriate value for $a\mathrm{TiO_2}$ (see Thomas & Watson, 2012; Wilson *et al*., 2012) and variations of Ti concentrations between sector zones in zircon (Chamberlain *et al*., 2014a). Two-feldspar thermometry (Chamberlain *et al*., 2014b) yields a ~80 °C range in model temperatures from Ig1Eb to Ig2Nc for the cores of crystals, somewhat less that the ~100 °C ranges from other phases, but indicating the

temperature zonation within the magma chamber prior to any changes associated with influx of the 'bright-rim' magma.

Use of Rhyolite-MELTS modelling on Bishop Tuff samples has been used to propose that the crystallisation temperature for Bishop Tuff crystals lies within a 10 °C range (Gualda *et al*., 2012a). The subsequent assertion from Rhyolite-MELTS modelling by Ghiorso & Gualda (2013) that the Bishop Fe–Ti-oxides are not in equilibrium is based on the relationship between calculated model temperatures and modelled $a\mathrm{TiO_2}$, which does not fall within a plausible pressure range as considered by them for the Bishop Tuff. Therefore it was asserted (following Lindsley *et al*., 1990, 1991; Frost & Lindsley, 1992) that the ilmenite in the Bishop Tuff is very late stage in origin and has not had a chance to equilibrate with magnetite (Ghiorso & Gualda, 2013). Three points suggest strongly, however, that such an argument is not soundly based. First, there is agreement in model temperatures and their ranges between two-feldspar thermometry, $\delta^{18}O$ thermometry and Fe–Ti-oxide thermometry. Second, given the demonstrably rapid timescales for equilibration of Fe–Ti-oxides with their host melt (Buddington & Lindsley, 1964; Hammond & Taylor, 1982; Ghiorso & Sack, 1991; Venezky & Rutherford, 1999), the systematic variations between model temperatures and minor element concentrations in both oxide phases (Hildreth, 1979), coupled with their generally euhedral shapes (indicating no widespread dissolution prior to eruption) it would seem most improbable that the magnetite and ilmenite are not in equilibrium (Evans & Bachmann, 2013; Evans *et al*., 2015). Third, Ghiorso & Gualda (2013) calculate temperature estimates for oxide pairs using the (equilibrium) model of Ghiorso & Evans (2008), yet the resulting derived values of $a\mathrm{TiO_2}$ are assumed to fall outside of their interpreted range for equilibrium pairs and hence to not represent equilibrium behaviour. However, the interpreted range for $a\mathrm{TiO_2}$ is not independently corroborated and therefore is to be a less rigorous test of equilibrium than others available (e.g. Mg-Mn exchange- Bacon & Hirschman, 1988). Our

886 conclusion is that the Fe–Ti-oxides were in equilibrium with the melt in which they were
887 erupted (see also Evans & Bachmann, 2013; Evans *et al*., 2015).
888
889 **One chamber or two?**
890 Recent studies have suggested a contrasting model to that in which the Bishop Tuff represents
891 tapping of a unitary zoned magma body (Hildreth, 1979; Wallace *et al*., 1999; Anderson *et*
892 *al*., 2000; Hildreth & Wilson, 2007). Instead it has been proposed by Gualda *et al*. (2012a),
893 Gualda & Ghiorso (2013a) and Gardner *et al*. (2014) that the Bishop Tuff is the product of
894 two laterally separated magma bodies, one feeding the early erupted, eastern material, and the
895 other feeding the late-erupted northern material, the latter with higher-Ba sanidine and
896 higher-Ca plagioclase, but with both bodies stored at similar temperatures and pressures.
897 Three lines of evidence were put forward in support of this two magma chamber hypothesis,
898 which we address here.
899 (1) A proposed lack of a thermal gradient in the pre-eruptive Bishop magma
900 chamber(s), with all modelled units having temperatures of 740 – 750 °C, according to
901 Rhyolite-MELTS model thermometry and experimental petrology (Gualda *et al*., 2012a;
902 Gualda & Ghiorso, 2013a; Gardener *et al*., 2014). However, as discussed above, we (and
903 other workers) find no evidence to suggest that the Fe–Ti oxides were not in equilibrium with
904 the magma that they were erupted with. Both the temperatures modelled from Fe–Ti oxide
905 compositions and those derived from all other mineral-specific methods yield estimates of a
906 ~100 °C gradient in temperature for the immediately pre-eruptive magma body. All mineral-
907 specific and isotopic data serve to highlight the thermally zoned nature of the Bishop magma
908 body.
909 (2) A proposed narrow range of pressures (175-200 MPa for all samples from the
910 Bishop Tuff) at which the eastern (early) and northern (late) magmas were stored before

911 eruption, based on Rhyolite-MELTS modelling and Si in glass barometry (Gualda & Ghiorso,
912 2013a, b). This narrow range in storage pressures is, however, not in agreement with data and
913 inferences made by earlier workers. In particular, studies of quartz-hosted melt inclusions
914 have shown a sequential change in inferred entrapment pressures, from ~160 MPa in the early
915 Bishop Tuff, to ~270 MPa in the late Bishop Tuff, the latter as inferred from melt inclusions
916 trapped in the bright-CL rims (Wallace *et al*., 1999; Peppard *et al*., 2001; Roberge *et al*.,
917 2013). This sequential change in entrapment pressure is mirrored by changes in both melt
918 inclusion and matrix glass compositions, again demonstrated by the matrix glass data
919 presented in this paper. The change from shallower entrapment depths to deeper entrapment
920 depths is not abrupt and in particular the intermediate entrapment pressures of 'middle-
921 erupted' eastern material (Ig2Ea) are identified by Wallace *et al*. (1999). In addition, simple
922 consideration of the volume of the Bishop Tuff divided by the area of the caldera ring fracture
923 yields an average estimate for drawdown in the magma chamber of 2.7 km (Hildreth &
924 Wilson, 2007), equivalent to an average ~60 MPa pressure difference between the earliest and
925 latest-erupted material. Given the inferences we derive in this paper for the stepped floor and
926 roof to the Bishop magma chamber, then this average pressure difference has to represent a
927 minimum value.
928 (3) An apparent bimodality in crystal compositions [plotted from Hildreth's (1977)
929 data], is used to suggest crystallisation in separate magma chambers (Gualda & Ghiorso,
930 2013a). This apparent bimodality, however, simply represents the influence of the 'bright-
931 rim' magma on the later erupted Bishop magma, and can be accurately replicated by core and
932 rim analyses from single crystals from single pumices in the northern-erupted units (e.g. Fig.
933 3). Field evidence also supports a single zoned magma chamber, with the systematic and
934 gradual changes from dominantly crystal-poor pumice in early units, to dominantly crystal-
935 rich pumice in late units (Wilson & Hildreth, 1997; Hildreth & Wilson, 2007), including the

mineralogically and geochemically intermediate transition zone that we recognise from our work.

Published evidence thus overwhelmingly implies that the Bishop Tuff eruption systematically tapped a unitary, gradationally zoned magma body. Why Rhyolite-MELTS-derived model-temperature estimates contrast so strongly with other thermometry methods raises questions about its applicability in this case, which could be related to values derived or adopted for $a\mathrm{TiO_2}$ and/or the model calibration. Rather than recalibrating MELTs over a wide spectrum of melt compositions, Gualda *et al*. (2012a) made small changes [comparable in magnitude to the fitting errors in the original MELTs calibration: Ghiorso & Sack (1995)] to the enthalpies of formation for quartz and the potassium end-member of alkali feldspar so that an early Bishop Tuff composition would have quartz, sanidine, and plagioclase on the liquidus. However this approach yields a temperature for early Bishop Tuff magma of ~760°C at 175 MPa and H_2O-saturated conditions, higher than the experimentally constrained temperature of <730°C at 200 MPa for the same melt composition (Scaillet & Hildreth, 2001). Gualda *et al*. (2012a) noted this discrepancy and stated that the offset was likely to be systematic. The absolute accuracy of temperatures calculated with Rhyolite-MELTS should therefore be viewed in this light. Furthermore, Rhyolite-MELTS, as an equilibrium thermodynamic model, is not applicable to samples that represent mixed magmas. Given the evidence for mixing with the 'bright-rim' magma (Figs. 4, 8, 9, 12, 13 and 14), Rhyolite-MELTS is unsuited for modelling temperatures and phase assemblages in matrix glass or bulk-rock compositions in the later-erupted Bishop Tuff.

The newly proposed silica-in-glass barometer (Gualda *et al*., 2013b) also gives similarly restricted ranges in storage pressures, but we consider these results to be overshadowed by dependence of the model on the precision of SiO_2 measurements (normally from EPMA). Typical values of 2 s.d. uncertainties vary from ± 0.6 wt.% SiO_2 (e.g. Wallace

961 *et al*., 1999; Bachmann *et al*., 2002; Allan, 2013) to ± 2.0 wt.% SiO_2 (Liu *et al*., 2006;
962 Cooper, 2014). For the former figure, the SiO_2-in-glass barometer yields approximate
963 differences in model pressures of ±50 MPa; for the glass data reported in this paper the
964 uncertainty of ±1.2 wt.% SiO_2 corresponds to a model pressure uncertainty of ±120 MPa.
965 Pressure differences of less than ~200 MPa are thus in essence unresolvable, given typical
966 uncertainties associated with matrix and melt inclusion glass analyses by EPMA.
967 Experimental results reported by Gardner et al. (2014) were also used by them to
968 assert that the 'Late Bishop Tuff magma body' had to be at a temperature of ≤740 °C, and
969 that higher model temperatures derived from the Fe-Ti oxides were in error. We would
970 suggest that such a conclusion is incorrect for two reasons. First, the bulk composition used in
971 their experiments was that of a whole-rock sample (which is itself a mixed magma) and does
972 not accurately reflect the melt composition of the later-erupted Bishop magma as indicated by
973 melt inclusion compositions (Wallace *et al*., 1999; Roberge *et al*., 2013). Second, most of the
974 experiments were carried out under water saturated conditions, despite the melt inclusion data
975 indicating that substantial amounts of CO_2 were present in the volatile phase and hence that
976 water activity would have been <1.0. Compositions of late Bishop Tuff melt inclusions are,
977 however, closely matched by a melt composition (AB401) used in the mixed-volatile
978 experiments of Klimm *et al*. (2008; see also Evans *et al.*, 2015). Their results show that for
979 this composition run under comparable water contents (3-4 wt %) and activities at a pressure
980 of 200 MPa, the three major phases quartz, plagioclase and sanidine are stable together up to
981 temperatures of 775 °C, and the experimental melt compositions under these conditions are a
982 very close match to those of the natural Bishop melt inclusions. Given that the experimental
983 melts do not vary widely with temperature and water content, we infer that at 200-275 MPa,
984 appropriate for the deeper parts of the Bishop magma body shortly before eruption, the match
985 would be as good.

COMPARISON AND CONTRASTS WITH OTHER SUPERVOLCANIC SYSTEMS

The work presented in this paper, combined with recent studies of the Bishop Tuff allows for comparisons and contrasts with other large-scale silicic eruptions (Table 7) to determine if common processes or timescales are present in these super-sized systems.

1). An underlying crystal-rich mush region is inferred to play varying roles in sourcing both melt and crystals into the overlying melt-dominant magma body (see Table 7; e.g. Wilson & Charlier, 2009; Allan *et al*., 2013; Cooper & Wilson, 2014) and in some cases can demonstrably be shown to be long-lived regions in the crust (Table 7). However, in the Bishop Tuff there are very few zircons with textures or ages appropriate to derivation from the Glass Mountain magma system (Chamberlain *et al*., 2014a). This observation highlights that either the underlying crystal mush was effectively reset, or that a completely new crystal mush system was established in the ~95 kyr time break between the youngest Glass Mountain and the climactic Bishop Tuff eruptions (Chamberlain *et al*., 2014a; Simon *et al*., 2014). The Bishop Tuff samples also show no clear evidence for texturally distinctive crystals that can be interpreted to have originated in a mushy region (cf. Bindeman *et al*., 2008; Allan *et al*., 2013).

2). A thermal and compositional gradient was largely established in the Bishop chamber prior to any mixing with the 'bright-rim' magma. The preservation of this gradient in systematic crystal and glass compositional variations shows that convection and mixing was not a significant chamber-wide process in the Bishop system, even though it is generally considered to be an inevitable consequence in such large bodies of thermally zoned magma [e.g. Huppert & Turner (1991) and references therein]. The volumetrically dominant upper part of the Bishop magma body thus conforms with the Hildreth (1979) concept of a body that was not convecting on any gross scale, and within which the associated crystal cargo

1011 grew as phenocrysts. The lower part of the Bishop magma body, in contrast, was undergoing
1012 mixing and associated convection, with incorporation of various components from the pre-
1013 existing Bishop magma and the incoming 'bright-rim' magma, and limited amounts of
1014 xenocrystic material [e.g. Triassic zircons: Chamberlain *et al*. (2014a)]. In contrast, magma
1015 bodies assembled as rapidly as the Oruanui, with associated high rates of heat input and
1016 output, show evidence for wholesale convection in their lack of systematic compositional
1017 zonation, and the diversity of crystal and melt-inclusion compositions found in single
1018 pumices (Liu *et al*., 2006; Wilson *et al*., 2006; Charlier *et al*., 2008; Allan, 2013; Allan *et al*.,
1019 2013).

1020 3). Zircon U-Pb age data imply that it took ~80 kyr to assemble the >600 km^3 melt-
1021 dominant Bishop magma body (Chamberlain *et al*., 2014a). There are no grounds for
1022 supposing that accumulation of this body was anything other than steady, based on the
1023 general textural uniformity of zircon grains (Chamberlain *et al*., 2014a), accompanying its
1024 proposed piecemeal assembly (Hildreth & Wilson, 2007). In other regions, the central Taupo
1025 Volcanic Zone (TVZ) of New Zealand especially, accumulation processes are an order of
1026 magnitude or more faster, reflecting the very high magma-related heat fluxes in the region,
1027 and commensurately rapid rates of heat loss via geothermal systems (Bibby *et al*., 1995;
1028 Wilson & Charlier, 2009: Table 7). At one extreme, the Oruanui eruption, broadly
1029 comparable in size to the Bishop Tuff, had its melt-dominant body assembled in <3000 years,
1030 and the underlying magmatic roots were wholly reorganised over a <~5000 year period into a
1031 new, highly productive system (Wilson & Charlier, 2009; Allan *et al*., 2013; Barker *et al*.,
1032 2014).

1033 4). There is a growing contrast between long-established precepts about the prolonged
1034 lengths of time required to develop large silicic magma bodies for eruption (e.g. Smith, 1979;
1035 Shaw, 1985; Trial & Spera, 1990; Reid, 2008) and data arising from studies involving dating

of eruptive components, especially U-Th disequilibrium and U-Pb dating of accessory phases (e.g. Vazquez & Reid, 2002, 2004; Simon & Reid, 2005; Bindeman *et al*., 2006, 2008; Wilson & Charlier, 2009; Chamberlain *et al*., 2014a). In part, these contrasts arise because different processes involved in magma generation and accumulation are being measured. The timescales required to physically accumulate an eruptible body of magma can, in cases like Taupo, be demonstrated to be 1-2 orders of magnitude shorter than the timescales recorded in ages of crystals that reflect the chemical processes that gave rise to those crystals and their associated magma composition (Sutton *et al*., 2000; Wilson & Charlier, 2009; Allan *et al*., 2013; Barker *et al*., 2014). The distinction is recognised at Taupo by the exceptionally frequent snapshots afforded of the magma system, contrasts in the zircon model-age spectra between closely spaced eruptions from the same magma system, and the systematic core-rim relationships in common mineral phases. In the Bishop Tuff, such a distinction is not feasible. The Bishop zircon age spectrum is almost entirely contained within the time gap since the last Glass Mountain eruption, and non-rimmed zircons from the early-erupted Bishop samples show no age or textural characteristics that would allow the contrast between growth in the mush versus growth in the melt-dominant body to be recognised. Overall, accumulation of the Bishop magma body is inferred by us to have occupied the ~80 kyr period indicated from the zircon age spectra, with input from the 'bright-rim' magma starting up to 10 kyr before eruption, and escalating in intensity ~500 yr before eruption (Chamberlain *et al*., 2014a, b). We would suggest that the shorter timescales proposed from Ti diffusion profiling in quartz (Gualda *et al*., 2012a) reflect the instability (i.e. growth and dissolution) of individual crystals in the later stages of accumulation of the melt-dominant body, not the growth of that body itself.

5). A subject of ongoing interest is the various triggering factors which have been proposed for large silicic systems. Saturation of the magma with volatiles is considered or

demonstrated to be the norm in large silicic systems (e.g. Dunbar & Hervig, 1992b; Stix & Layne, 1996; Wallace *et al*., 1999; Liu *et al*., 2006; Chesner & Luhr, 2010; Fowler & Spera, 2010), so that volatile saturation in itself cannot be a sole trigger for eruption onset (cf. Blake, 1984). Although intrusion of a more mafic magma, or buoyancy-driven overpressure of such a large volume of magma are often suggested as critical triggers for eruption (e.g. Sparks *et al*., 1977; Caricchi *et al*., 2014; Malfait *et al*., 2014), recent studies have highlighted a role for external tectonic forces in both triggering and halting supereruptions (e.g. Allan *et al*., 2012; Cooper *et al*., 2012). Although our work has not found evidence in the crystal-specific record to support or disprove this hypothesis for the Bishop Tuff, it would appear that the longer timescales of mixing with the 'bright-rim' magma (Chamberlain *et al*., 2014a, b) are too extended to represent a direct trigger as has been suggested by Wark *et al*. (2007). However, recent volcanism in Long Valley has been shown to be closely linked to faulting (e.g. Bursik *et al*., 2003), and therefore it seems plausible that tectonic processes may have allowed or aided rise of the 'bright-rim' magma and contributed to triggering of the Bishop Tuff eruption itself. Whether the paleotectonic record could be probed in enough detail to investigate this hypothesis is unknown, but it represents a possible avenue for further exploration in the Long Valley region.

CONCLUSIONS

We reach four main conclusions relating to the pre-eruptive Bishop Tuff magma chamber and its relationship to rejuvenating magmatism.

1. Our data confirm that there was a single, unitary Bishop Tuff magma chamber that was stratified in temperature and composition even prior to intrusion of the 'bright-rim' magma. Available evidence strongly counts against proposals for the presence of two

laterally separated magma chambers at similar depths and temperatures feeding the early and late Bishop Tuff, respectively.

2. The stratification of the Bishop magma chamber was gradational from the upper parts (contributing to earlier-erupted deposits) yielding the most-evolved glass compositions, unzoned phenocrysts, pyroxene-free and lower model temperatures through to lower parts (dominating late-erupted deposits) with less-evolved glass compositions, systematically zoned sanidine and quartz phenocrysts, pyroxene-bearing and higher model temperatures (Figs. 4-8). There is an intervening transition zone between the dominant ~2/3 volume of more-evolved and the subordinate ~1/3 volume of less-evolved compositions. The transitional magma is represented in samples from the Sherwin lobe of Ig1Eb and Ig2Na which show mineralogical and geochemical characteristics in common with both earlier (eastern) and later (northern) erupted compositions.

3. We find no evidence that significant amounts of eastern-type magma were ever present prior to the eruption in the chamber below the northern vents of the Bishop eruption (Fig. 14). Similarly, there is a sparseness of xr less-evolved magma vented from the southerly and easterly parts of the caldera. We thus infer that there was an asymmetric roof and floor to the magma body, both stepped down to the north (Fig. 14), the former as previously proposed from melt inclusion studies.

4. From their significant enrichment in Ba, Sr, LREE and Ti (Fig. 9), the sparse dacitic clasts and dark pumices are confirmed as possible analogues for the ‘bright-rim’ magma that intruded the lower regions of the Bishop magma chamber .The ‘bright-rim’ magma cannot be represented by a single composition, however, and instead likely represents varied tappings of a chemically heterogeneous source. Its interaction with the pre-existing Bishop magma body was prolonged over hundreds to thousands of years, and affected

through mixing the lower ~1/3 by volume of an otherwise stably stratified and non-convecting body of crystal-poor rhyolite

ACKNOWLEDGEMENTS

We thank Wes Hildreth, John Gamble, John Wolff, Pat Browne and Joel Baker for valuable discussions, advice and comments, and Aidan Allan, Simon Barker, George Cooper, Monica Handler and Richard Wysoczanski for assistance with laboratory studies at various stages of this work. Constructive reviews from Madeleine Humphreys, John Wolff and Mary Reid led to improvements of this manuscript. Wendy Bohrson is thanked for her review and editorial handling.

FUNDING

KJC acknowledges with thanks the receipt of a New Zealand International Doctoral Research Scholarship, administered by Education New Zealand. We also acknowledge generous support from the Marsden Fund (grant VUW0813) and award of a James Cook Fellowship to CJNW, both administered by the Royal Society of New Zealand. Fieldwork by KJC was partially supported by a Kleinman Award, administered by the U.S. Geological Survey and by grants from the Faculty of Science at Victoria University.

REFERENCES

Allan, A. S. R. (2013). The Oruanui eruption: insights into the generation and dynamics of the world's youngest supereruption. [Ph.D. Thesis] Victoria University of Wellington, New Zealand.

Allan, A. S. R., Wilson, C. J. N., Millet, M. -A. & Wysoczanski, R. J. (2012). The invisible hand: tectonic triggering and modulation of a rhyolitic supereruption. *Geology* **40**, 563-566.

1135 Allan, A. S. R., Morgan, D. J., Wilson, C. J. N. & Millet, M. -A. (2013). From mush to
1136 eruption in centuries: assembly of the super-sized Oruanui magma body. *Contributions*
1137 *to Mineralogy and Petrology* **166**, 143-164.
1138 Andersen, D. J. & Lindsley, D. H. (1988). Internally consistent solution models for Fe-Mg-
1139 Mn-Ti oxides: Fe-Ti oxides. *American Mineralogist* **73**, 714-726.
1140 Anderson, A. T., Davis, A. M. & Lu, F. (2000). Evolution of Bishop Tuff rhyolitic magma
1141 based on melt and magnetite inclusions and zoned phenocrysts. *Journal of Petrology*
1142 **41**, 449-473.
1143 Bachmann, O. & Bergantz, G. W. (2004). On the origin of crystal-poor rhyolites: extracted
1144 from batholithic crystal mushes. *Journal of Petrology* **45**, 1565-1582.
1145 Bachmann, O., Dungan, M. A. & Lipman, P. W. (2002). The Fish Canyon magma body, San
1146 Juan Volcanic Field, Colorado: Rejuvenation and eruption of an upper-crustal batholith.
1147 *Journal of Petrology* **43**, 1469-1503.
1148 Bacon, C. R. & Hirschmann, M. M. (1988). Mg/Mn partitioning as a test for equilibrium
1149 between coexisting Fe-Ti oxides. *American Mineralogist* **73**, 57-61.
1150 Bacon, C. R. & Lowenstern, J. B. (2005). Late Pleistocene granodiorite source for recycled
1151 zircon and phenocrysts in rhyodacite lava at Crater Lake, Oregon. *Earth and Planetary*
1152 *Science Letters* **233**, 277-293.
1153 Bailey, R. A. (1989). Geologic map of Long Valley caldera, Mono Inyo Craters volcanic
1154 chain and vicinity, eastern California. *US Geological Survey Miscellaneous*
1155 *Investigations Series Map* **I-1933**, scale 1:62 500.
1156 Bailey, R. A. (2004). *Eruptive history and chemical evolution of the precaldera and*
1157 *postcaldera basalt-dacite sequences, Long Valley, California: Implications for magma*
1158 *sources, current seismic unrest, and future volcanism*. *U.S. Geological Survey*
1159 *Professional Papers* **1692**, 1-75.
1160 Bailey, R. A., Dalrymple, G. B. & Lamphere, M. A. (1976). Volcanism, structure, and
1161 geochronology of Long Valley Caldera, Mono County, California. *Journal of*
1162 *Geophysical Research* **81**, 725-744.
1163 Barker, S. J., Wilson, C. J. N., Smith, E. G. C., Charlier, B. L. A., Wooden, J. L., Hiess, J. &
1164 Ireland, T. R. (2014). Post-supereruption magmatic reconstruction of Taupo volcano
1165 (New Zealand), as reflected in zircon ages and trace elements. *Journal of Petrology* **55**,
1166 1511-1533.

1167 Bibby, H. M., Caldwell, T. G., Davey, F. J. & Webb, T. H. (1995). Geophysical evidence on
1168 the structure of the Taupo Volcanic Zone and its hydrothermal circulation. *Journal of*
1169 *Volcanology and Geothermal Research* **68**, 29-58.
1170 Bindeman, I. N. & Valley, J. W. (2002). Oxygen isotope study of the Long Valley magmatic
1171 system, California: isotope thermometry and convection in large silicic magma bodies.
1172 *Contributions to Mineralogy and Petrology* **144**, 185-205.
1173 Bindeman, I. N., Valley, J. W., Wooden, J. L. & Persing, H. M. (2001). Post-caldera volcanism: in
1174 situ measurement of U–Pb age and oxygen isotope ratio in Pleistocene zircons from
1175 Yellowstone caldera. *Earth and Planetary Science Letters* **189**, 197-206.
1176 Bindeman, I. N., Schmitt, A. K. & Valley, J. W. (2006). U-Pb geochronology of silicic tuffs from the
1177 Timber Mountain/Oasis Valley caldera complex, Nevada: rapid generation of large volume
1178 magmas by shallow-level remelting. *Contributions to Mineralogy and Petrology* **152**, 649-665.
1179 Bindeman, I. N., Fu, B., Kita, N. T. & Valley, J. W. (2008). Origin and evolution of silicic
1180 magmatism at Yellowstone based on ion microprobe analysis of isotopically zoned zircons.
1181 *Journal of Petrology* **49**, 163-193.
1182 Blake, S. (1984). Volatile oversaturation during the evolution of silicic magma chambers as
1183 an eruption trigger. *Journal of Geophysical Research* **89**, 8237-8244.
1184 Brophy, J. G., Ota, T., Kunihiro, T., Tsujimori, T. & Nakamaru, E. (2011). In situ ion-
1185 microprobe determination of trace element partition coefficients for hornblende,
1186 plagioclase, orthopyroxene, and apatite in equilibrium with natural rhyolitic glass, Little
1187 Glass Mountain Rhyolite, California. *American Mineralogist* **96**, 1838-1850.
1188 Brown, S. J. A. & Fletcher, I. R. (1999). SHRIMP U-Pb dating of the preeruption growth
1189 history of zircons from the 340 ka Whakamaru Ignimbrite, New Zealand: Evidence for
1190 >250 ky magma residence times. *Geology* **27**, 1035-1038.
1191 Brown, S. J. A., Wilson, C. J. N., Cole, J. W. & Wooden, J. (1998). The Whakamaru group
1192 ignimbrites, Taupo Volcanic Zone, New Zealand: evidence for reverse tapping of a
1193 zoned silicic magmatic system. *Journal of Volcanology and Geothermal Research* **84**,
1194 1-37.
1195 Buddington, A. F. & Lindsley, D. H. (1964): Iron-titanium oxide minerals and synthetic
1196 equivalents. *Journal of Petrology* **5**, 310-357.
1197 Bursik, M. I., Renshaw, C., McCalpin, J. & Berry, M. (2003). A volcanotectonic cascade:
1198 activation of range front faulting and eruptions by dike intrusion, Mono Basin-Long
1199 Valley caldera, California. *Journal of Geophysical Research* **108**, 2393.

Caricchi, L., Annen, C., Blundy, J., Simpson, G. & Pinel, V. (2014). Frequency and magnitude of volcanic eruptions controlled by magma injection and buoyancy. *Nature Geoscience* **7**, 126-130.

Chamberlain, K. J., Wilson, C. J. N., Wooden, J. L., Charlier, B. L. A. & Ireland, T. R. (2014a). New perspectives on the Bishop Tuff from zircon textures, ages and trace elements. *Journal of Petrology* **55**, 395-426.

Chamberlain, K. J., Morgan, D. J. & Wilson, C. J. N. (2014b). Timescales of mixing and mobilisation in the Bishop Tuff magma body: perspectives from diffusion chronometry. *Contributions to Mineralogy and Petrology* **168**, 1034.

Charlier, B. L. A., Wilson, C. J. N., Lowenstern, J. B., Blake, S., van Calsteren, P. W. & Davidson, J. P. (2005). Magma generation at a large, hyperactive silicic volcano (Taupo, New Zealand) revealed by U–Th and U–Pb systematics in zircons. *Journal of Petrology* **46**, 3-32.

Charlier, B. L. A., Wilson, C. J. N. & Davidson, J. P. (2008). Rapid open-system assembly of a large silicic magma body: time-resolved evidence from cored plagioclase crystals in the Oruanui eruption deposits, New Zealand. *Contributions to Mineralogy and Petrology* **156**, 799-813.

Chesner, C. A. & Luhr, J. F. (2010). A melt inclusion study of the Toba Tuffs, Sumatra, Indonesia. *Journal of Volcanology and Geothermal Research* **197**, 259-278.

Christensen, J. N. & DePaolo, D. J. (1993). Time scales of large volume silicic magma systems- Sr isotopic systematics of phenocrysts and glass from the Bishop Tuff, Long Valley, California. *Contributions to Mineralogy and Petrology* **113**, 100-114.

Christensen, J. N. & Halliday, A. N. (1996). Rb-Sr ages and Nd isotopic compositions of melt inclusions from the Bishop Tuff and the generation of silicic magma. *Earth and Planetary Science Letters* **144**, 547-561.

Cooper, G. F. (2014). The dynamics of large-scale silicic magmatic systems: case studies from Mangakino Volcanic Centre, Taupo Volcanic Zone, New Zealand. [Ph. D. Thesis] Victoria University of Wellington, New Zealand.

Cooper, G. F. & Wilson, C. J. N. (2014). Development, mobilisation and eruption of a large crystal-rich rhyolite: the Ongatiti ignimbrite, New Zealand. *Lithos* **198-199**, 38-57.

Cooper, G. F., Wilson, C. J. N., Millet, M.-A., Baker, J. A. & Smith, E. G. C. (2012). Systematic tapping of independent magma chambers during the 1 Ma Kidnappers supereruption. *Earth and Planetary Science Letters* **313-314**, 23-33.

Cooper, G. F., Wilson, C. J. N., Charlier, B. L. A., Wooden, J. L. & Ireland, T. R. (2014). Temporal evolution and compositional signatures of two supervolcanic systems recorded in zircons from Mangakino volcanic centre, New Zealand. *Contributions to Mineralogy and Petrology* **167**, 1018.

Davies, G. R. & Halliday, A. N. (1998). Development of the Long Valley rhyolitic magma system: strontium and neodymium isotope evidence from glasses and individual phenocrysts. *Geochimica et Cosmochimica Acta* **62**, 3561-3574.

Dunbar, N. W. & Hervig, R. L. (1992a). Petrogenesis and volatile stratigraphy of the Bishop Tuff: evidence from melt inclusion analysis. *Journal of Geophysical Research* **97**, 15129-15150.

Dunbar, N. W. & Hervig, R. L. (1992b). Volatile and trace element composition of melt inclusions from the lower Bandelier Tuff: implications for magma chamber processes and eruptive style. *Journal of Geophysical Research* **97**, 15151-15170.

Evans, B. W. & Bachmann, O. (2013). Implications of equilibrium and disequilibrium among crystal phases in the Bishop Tuff. *American Mineralogist* **98**, 271-274.

Evans, B. W., Hildreth, W., Scaillet, B. & Bachmann, O. (2014). On the continuity and correlation of phase compositions and temperatures in the Bishop Tuff. *American Mineralogist* (in review).

Frost, B. R. & Lindsley, D. H. (1992). Equilibria among Fe-Ti oxides, pyroxenes, olivine, and quartz. Part II. Application. *American Mineralogist* **77**, 1004-1020.

Gardner, J. E., Befus, K. S., Gualda, G. A. R. & Ghiorso, M. S. (2014). Experimental constraints on rhyolite-MELTS and the Late Bishop Tuff magma body. *Contributions to Mineralogy and Petrology* **168**, 1051.

Ghiorso, M. S. & Evans, B. W. (2008). Thermodynamics of rhombohedral oxide solid solutions and a revision of the Fe-Ti two-oxide geothermometer and oxygen-barometer. *American Journal of Science* **308**, 957-1039.

Ghiorso, M. S. & Gualda, G. A. R. (2013). A method for estimating the activity of titania in magmatic liquids from the compositions of coexisting rhombohedral and cubic iron-titanium oxides. *Contributions to Mineralogy and Petrology* **165**, 73-81.

Ghiorso, M. S. & Sack, R. O. (1991). Fe-Ti oxide geothermometry: thermodynamic formulation and the estimation of intensive variable in silicic magmas. *Contributions to Mineralogy and Petrology* **108**, 485-510.

Ghiorso, M. S. & Sack, R. O. (1995). Chemical mass-transfer in magmatic processes. 4. A revised and internally consistent thermodynamic model for the interpolation and

1267 extrapolation of liquid-solid equilibria in magmatic systems at elevated temperatures
1268 and pressures. *Contributions to Mineralogy and Petrology* **119**, 197-212.
1269 Goff, F., Warren, R. G., Goff, C. J. & Dunbar, N. (2014). Eruption of reverse-zoned upper
1270 Tshirege Member, Bandelier Tuff from centralized vents within Valles caldera, New
1271 Mexico. *Journal of Volcanology and Geothermal Research* **276**, 82-104.
1272 Gravley, D. M., Wilson, C. J. N., Leonard, G. S. & Cole, J. W. (2007). Double trouble: paired
1273 ignimbrite eruptions and collateral subsidence in the Taupo Volcanic Zone, New
1274 Zealand. *Geological Society of America Bulletin* **119**, 18-30.
1275 Gualda, G. A. R. (2007). Crystal and bubble populations in the early-erupted Bishop rhyolitic
1276 magma: Microscopy, x-ray tomography and microanalysis of pumice clasts. [Ph.D.
1277 Thesis]: The University of Chicago, Chicago, Illinois.
1278 Gualda, G. A. R. & Ghiorso, M. S. (2013a). The Bishop Tuff giant magma body: an
1279 alternative to the Standard Model. *Contributions to Mineralogy and Petrology* **166**,
1280 755-775.
1281 Gualda, G. A. R. & Ghiorso, M. S. (2013b). Low-pressure origin of high-silica rhyolites and
1282 granites. *Journal of Geology* **121**, 537-545.
1283 Gualda, G. A. R., Ghiorso, M. S., Lemons, R. V. & Carley, T. L. (2012a). Rhyolite-MELTS:
1284 a modified calibration of MELTS optimized for silica-rich, fluid-bearing magmatic
1285 systems. *Journal of Petrology* **53**, 875-890.
1286 Gualda, G. A. R., Pamukcu, A. S., Ghiorso, M. S., Anderson, A. T., Sutton, S. R. & Rivers,
1287 M. L. (2012b). Timescales of quartz crystallization and the longevity of the Bishop
1288 giant magma body. *PLoS ONE* **7**, e37492.
1289 Halliday, A. N., Fallick, A. E., Hutchinson, J. & Hildreth, W. (1984). A Nd, Sr and O isotopic
1290 investigation into the causes of chemical and isotopic zonation in the Bishop Tuff,
1291 California. *Earth and Planetary Science Letters* **68**, 379-391.
1292 Halliday, A. N., Mahood, G. A., Holden, P., Metz, J. M., Dempster, T. J. & Davidson, J. P.
1293 (1989). Evidence for long residence times of rhyolitic magma in the Long Valley
1294 magmatic system: the isotopic record in precaldera lavas of Glass Mountain. *Earth and*
1295 *Planetary Science Letters* **94**, 274-290.
1296 Hammond, P. A. & Taylor, L. A. (1982). The ilmenite/titano-magnetite assemblage: kinetics
1297 of re-equilibration. *Earth and Planetary Science Letters* **61**, 143-150.
1298 Hervig, R. L. & Dunbar, N. (1992). Causes of chemical zoning in the Bishop (California) and
1299 Bandelier (New Mexico) magma chambers. *Earth and Planetary Science Letters* **111**,
1300 97-108.

1301 Hildreth, E. W. (1977). The magma chamber of the Bishop Tuff: Gradients in temperature,
1302 pressure, and composition [Ph. D. Thesis]: University of California, Berkeley.
1303 Hildreth, W. (1979). The Bishop Tuff: evidence for the origin of compositional zonation in
1304 silicic magma chambers. In: Chapin, C. E. & Elston, W. E. (eds.) *Ash-flow tuffs*.
1305 *Geological Society of America Special Papers* **180**, 43-75.
1306 Hildreth, W. (2004). Volcanological perspectives on Long Valley, Mammoth Mountain, and
1307 Mono Craters: several contiguous but discrete systems. *Journal of Volcanology and*
1308 *Geothermal Research* **136**, 169-198.
1309 Hildreth, W. & Mahood, G. A. (1986). Ring-fracture eruption of the Bishop Tuff. *Geological*
1310 *Society of America Bulletin* **97**, 396-403.
1311 Hildreth, W. & Wilson, C. J. N. (2007). Compositional zoning of the Bishop Tuff. *Journal of*
1312 *Petrology* **48**, 951-999.
1313 Huppert, H. E. & Turner, J. S. (1991). Comments on: 'On convective style and vigor in sheet-
1314 like magma chambers' by Bruce D. Marsh. *Journal of Petrology* **32**, 851-854.
1315 Klimm, K., Holtz, F. & King, P. L. (2008). Fractionation vs. magma mixing in the Wangrah
1316 Suite A-type granites, Lachlan Fold Belt, Australia: experimental constraints. *Lithos*
1317 **102**, 415-434.
1318 Lindsley, D. H., Frost, B. R., Andersen, D. J. & Davidson, P. J. (1990). Fe-Ti oxide-silicate
1319 equilibria: assemblages with orthopyroxene. In R. Spencer, I. & Chou, I. (eds), *Fluid-*
1320 *mineral interactions: A tribute to H.P. Eugster*. *Geochemical Society Special*
1321 *Publication* **2**, 103–119.
1322 Lindsley, D. H., Frost, B. R., Ghiorso, M. S. & Sack, R. O. (1991) Oxides lie: the Bishop
1323 Tuff did not erupt from a thermally zoned magma body. *EOS, Transactions of the*
1324 *American Geophysical Union* **72**, 313.
1325 Liu, Y., Anderson, A. T., Wilson, C. J. N., Davis, A. M., & Steele, I. M. (2006). Mixing and
1326 differentiation in the Oruanui rhyolitic magma, Taupo, New Zealand: evidence from
1327 volatiles and trace elements in melt inclusions. *Contributions to Mineralogy and*
1328 *Petrology* **151**, 71-87.
1329 Lu, F., Anderson, A. T. & Davis, A. M. (1992). Melt inclusions and crystal-liquid separation
1330 in rhyolitic magma of the Bishop Tuff. *Contributions to Mineralogy and Petrology* **110**,
1331 113-120.
1332 Malfait, W., Seifert, R., Petitgirard, S., Perrillat, J. -P., Mezouar, M., Ota, T., Nakamura, E.,
1333 Lerch, P. & Sanchez-Valle, C. (2014). Supervolcano eruptions driven by melt buoyancy
1334 in large silicic chambers. *Nature Geoscience* **7**, 122-125.

1335 Matthews, N. E., Huber, C., Pyle, D. M. & Smith, V. C. (2012a). Timescales of magma
1336 recharge and reactivation of large silicic systems from Ti diffusion in quartz. *Journal of*
1337 *Petrology* **53**, 1385-1416.
1338 Matthews, N. E., Pyle, D. M., Smith, V. C., Wilson, C. J. N., Huber, C. & Van Hinsberg, V.
1339 (2012b). Quartz zoning and the pre-eruptive evolution of the~ 340-ka Whakamaru
1340 magma systems, New Zealand. *Contributions to Mineralogy and Petrology* **163**, 87-
1341 107.
1342 Metz, J. M. & Bailey, R. A. (1993). Geologic map of Glass Mountain, Mono County,
1343 California. *U.S. Geological Survey Miscellaneous Investigation Series Map* **I-1995**,
1344 scale 1:24 000.
1345 Metz, J. M. & Mahood, G. A. (1985). Precursors to the Bishop Tuff eruption: Glass
1346 Mountain, Long Valley, California. *Journal of Geophysical Research* **90**, 11121-11126.
1347 Metz, J. M. & Mahood, G. A. (1991). Development of the Long Valley, California, magma
1348 chamber recorded in precaldera rhyolite lavas of Glass Mountain. *Contributions to*
1349 *Mineralogy and Petrology* **106**, 379-397.
1350 Miller, C. F. & Wark, D. A. (2008). Supervolcanoes and their explosive supereruptions.
1351 *Elements* **4**, 11-15.
1352 Miller, J. S., Matzel, J. E. P., Miller, C. F., Burgess, S. D. & Miller, R. B. (2007). Zircon
1353 growth and recycling during the assembly of large, composite arc plutons. *Journal of*
1354 *Volcanology and Geothermal Research* **167**, 282–299.
1355 Naney, M. T. (1983). Phase equilibria of rock-forming ferromagnesian silicates in granitic
1356 systems. *American Journal of Science* **283**, 993-1033.
1357 Olin, P. H. & Wolff, J. A. (2010). Rare earth and high field strength element partitioning
1358 between iron-rich clinopyroxenes and felsic liquids. *Contributions to Mineralogy and*
1359 *Petrology* **160**, 761-775.
1360 Pamukcu, A. S., Gualda, G. A. R. & Anderson, A. T. (2012). Crystallization stages of the
1361 Bishop Tuff magma body recorded in crystal textures in pumice clasts. *Journal of*
1362 *Petrology* **53**, 589-609.
1363 Peppard, B. T., Steele, I. M., Davis, A. M., Wallace, P. J. & Anderson, A. T. (2001). Zoned
1364 quartz phenocrysts from the rhyolitic Bishop Tuff. *American Mineralogist* **86**, 1034-
1365 1052.
1366 Rampino, M. R. & Self, S. (1993). Climate-volcanism feedback and the Toba eruption of
1367 ~74,000 years ago. *Quaternary Research* **40**, 269-280.
1368 Reid, M. R. (2008). How long does it take to supersize an eruption? *Elements* **4**, 23-28.

1369 Reid, M. R. & Coath, C. D. (2000). In situ U-Pb ages of zircons from the Bishop Tuff: no
1370 evidence for long crystal residence times. *Geology* **28**, 443-446.
1371 Reid, M. R., Vazquez, J. A. & Schmitt, A. K. (2011). Zircon-scale insights into the history of
1372 a supervolcano, Bishop Tuff, Long Valley, California, with implications for the Ti-in-
1373 zircon geothermometer. *Contributions to Mineralogy and Petrology* **161**, 293-311.
1374 Rivera, T. A., Storey, M., Zeeden, C., Hilgen, F. J. & Kuiper, K. (2011). A refined
1375 astronomically calibrated $^{40}Ar/^{39}Ar$ age for Fish Canyon sanidine. *Earth and Planetary*
1376 *Science Letters* **311**, 420-426.
1377 Roberge, J., Wallace, P. J. & Kent, A. J. R. (2013). Magmatic processes in the Bishop Tuff
1378 rhyolitic magma based on trace elements in melt inclusions and pumice matrix glass.
1379 *Contributions to Mineralogy and Petrology* **165**, 237-257.
1380 Sarna-Wojcicki, A. M., Reheis, M. C., Pringle, M. S., Fleck, R. J., Burbank, D. W., Meyer, C.
1381 E., Slate, J. L., Wan, E., Budahn, J. R., Troxel, B. & Walker, J. P. (2005). *Tephra layers*
1382 *of Blind Spring Valley and related upper Pliocene and Pleistocene tephra layers,*
1383 *California, Nevada, and Utah: isotopic ages, correlation, and magnetostratigraphy*.
1384 *United States Geological Survey Professional Paper* **1701**, 1-63.
1385 Scaillet, B. & Hildreth, W. (2001). Experimental constraints on the origin and evolution of
1386 the Bishop Tuff. Abstract for presentation at the Penrose Conference on Longevity and
1387 Dynamics of Rhyolitic Magma Systems, Mammoth Lakes, California, June 7-12, 2001.
1388 URL: http://hal.archives-ouvertes.fr/docs/00/10/26/16/PDF/Abstract_Penrose-1.pdf
1389 Self, S. (2006). The effects and consequences of very large explosive volcanic eruptions.
1390 *Philosophical Transactions of the Royal Society, London* **A364**, 2073-2097.
1391 Self, S. & Blake, S. (2008). Consequences of explosive supereruptions. *Elements* **4**, 41-46.
1392 Shane, P., Nairn, I. A. & Smith, V. C. (2005). Magma mingling in the ~50 ka Rotoiti eruption
1393 from Okataina Volcanic Centre: implications for geochemical diversity and chronology
1394 of large volume rhyolites. *Journal of Volcanology and Geothermal Research* **139**, 295-
1395 313.
1396 Shaw, H. R. (1985). Links between magma-tectonic rate balances, plutonism, and volcanism.
1397 *Journal of Geophysical Research* **90**, 11275-11288.
1398 Simon, J. I. & Reid, M. R. (2005). The pace of rhyolite differentiation and storage in an
1399 'archetypical' silicic magma system, Long Valley, California. *Earth and Planetary*
1400 *Science Letters* **235**, 123-140.

1401 Simon, J. I., Reid, M. R. & Young, E. D. (2007). Lead isotopes by LA-MC-ICPMS: tracking
1402 the emergence of mantle signatures in an evolving silicic magma system. *Geochimica et*
1403 *Cosmochimica Acta* **71**, 2014-2035.
1404 Simon, J. I., Weis, D., DePaolo, D. J., Renne, P. R., Mundil, R. & Schmitt, A. K. (2014).
1405 Assimilation of preexisting Pleistocene intrusions at Long Valley by periodic magma
1406 recharge accelerates rhyolite generation: rethinking the remelting model. *Contributions*
1407 *to Mineralogy and Petrology* **167**, 955.
1408 Smith, R. L. (1979). Ash-flow magmatism. In: Chapin, C. E. & Elston, W. E. (eds) *Ash-flow*
1409 *Tuffs*. *Geological Society of America Special Papers* **180**, 5-27.
1410 Sparks, R. S. J., Self, S., Grattan, J. P., Oppenheimer, C., Pyle, D. M. & Rymer, H. (2005).
1411 *Super-eruptions: global effects and future threats*. Report of a Geological Society of
1412 London working group. London, UK: The Geological Society, 24 p.
1413 Sparks, R. S. J., Sigurdsson, H. & Wilson, L. (1977). Magma mixing: a mechanism for
1414 triggering acid explosive eruptions. *Nature* **267**, 315-318.
1415 Stix, J. & Layne, G. D. (1996). Gas saturation and evolution of volatile and light lithophile
1416 elements in the Bandelier magma chamber between two caldera-forming eruptions.
1417 *Journal of Geophysical Research* **101**, 25181-25196.
1418 Sutton, A. N., Blake, S., Wilson, C. J. N. & Charlier, B. L. A. (2000). Late Quaternary evolution of a
1419 hyperactive rhyolite magmatic system: Taupo volcanic centre, New Zealand. *Journal of the*
1420 *Geological Society, London* **157**, 537-552.
1421 Thomas, J. B. & Watson, E. B. (2012). Application of the Ti-in-quartz thermobarometer to
1422 rutile-free systems. Reply to: a comment on: 'TitaniQ under pressure: the effect of
1423 pressure and temperature on the solubility of Ti in quartz' by Thomas et al.
1424 *Contributions to Mineralogy and Petrology* **164**, 369-374.
1425 Thomas, J. B., Watson, E. B., Spear, F. S., Shemella, P. T., Nayak, S. K. & Lanzirotti, A.
1426 (2010). TitaniQ under pressure: the effect of pressure and temperature on the solubility
1427 of Ti in quartz. *Contributions to Mineralogy and Petrology* **160**, 743-759.
1428 Trial, A. F. & Spera, F. J. (1990). Mechanisms for the generation of compositional
1429 heterogeneities in magma chambers. *Geological Society of America Bulletin* **102**, 353-
1430 367.
1431 Vazquez, J. A. & Reid, M. R. (2002). Time scales of magma storage and differentiation of
1432 voluminous high-silica rhyolites at Yellowstone caldera, Wyoming. *Contributions to*
1433 *Mineralogy and Petrology* **144**, 274-285.

1434 Vazquez, J. A. & Reid, M. R. (2004). Probing the accumulation history of the voluminous
1435 Toba magma. *Science* **305**, 991-994.
1436 Venezky, D. Y. & Rutherford, M. J. (1999). Petrology and Fe-Ti oxide reequilibration of the
1437 1991 Mount Unzen mixed magma. *Journal of Volcanology and Geothermal Research*
1438 **89**, 213-230.
1439 Wallace, P. J., Anderson, A. T. & Davis, A. M. (1995). Quantification of pre-eruptive
1440 exsolved gas contents in silicic magma. *Nature* **377**, 612-616.
1441 Wallace, P. J., Anderson, A. T. & Davis, A. M. (1999). Gradients in H_2O, CO_2, and exsolved
1442 gas in a large-volume silicic magma system: Interpreting the record preserved in melt
1443 inclusions from the Bishop Tuff. *Journal of Geophysical Research* **104**, 20097-20122.
1444 Wark, D. A., Hildreth, W., Spear, F. S., Cherniak, D. J. & Watson, E. B. (2007). Pre-eruption
1445 recharge of the Bishop magma system. *Geology* **35**, 235-238.
1446 Wilcock, J., Goff, F., Minarik, W. G. & Stix, J. (2013). Magmatic recharge during the
1447 formation and resurgence of the Valles caldera, New Mexico, USA: evidence from
1448 quartz compositional zoning and geothermometry. *Journal of Petrology* **54**, 635-664.
1449 Wilson, C. J. N. & Charlier, B. L. A. (2009). Rapid rates of magma generation at
1450 contemporaneous magma systems, Taupo volcano, New Zealand: insights from U-Th
1451 model-age spectra in zircons. *Journal of Petrology* **50**, 875-907.
1452 Wilson, C. J. N. & Hildreth, W. (1997). The Bishop Tuff: new insights from eruptive
1453 stratigraphy. *Journal of Geology* **105**, 407-439.
1454 Wilson, C. J. N., Blake, S., Charlier, B. L. A. & Sutton, A. N. (2006). The 26·5 ka Oruanui
1455 eruption, Taupo volcano, New Zealand: development, characteristics and evacuation of
1456 a large rhyolitic magma body. *Journal of Petrology* **47**, 35-69.
1457 Wilson, C. J. N., Seward, T. M., Charlier, B. L. A., Allan, A. S. R. & Bello, L. (2012). A
1458 comment on: 'TitaniQ under pressure: the effect of pressure and temperature on the
1459 solubility of Ti in quartz', by Jay B. Thomas, E. Bruce Watson, Frank S. Spear, Philip
1460 T. Shemella, Saroj K. Nayak and Antonio Lanzirotti. *Contributions to Mineralogy and*
1461 *Petrology* **164**, 359-368.
1462 Wolff, J. A. & Ramos, F. C. (2003). Pb isotope variations among Bandelier Tuff feldspars:
1463 No evidence for a long-lived silicic magma chamber. *Geology* **31**, 533-536.
1464

FIGURES AND CAPTIONS

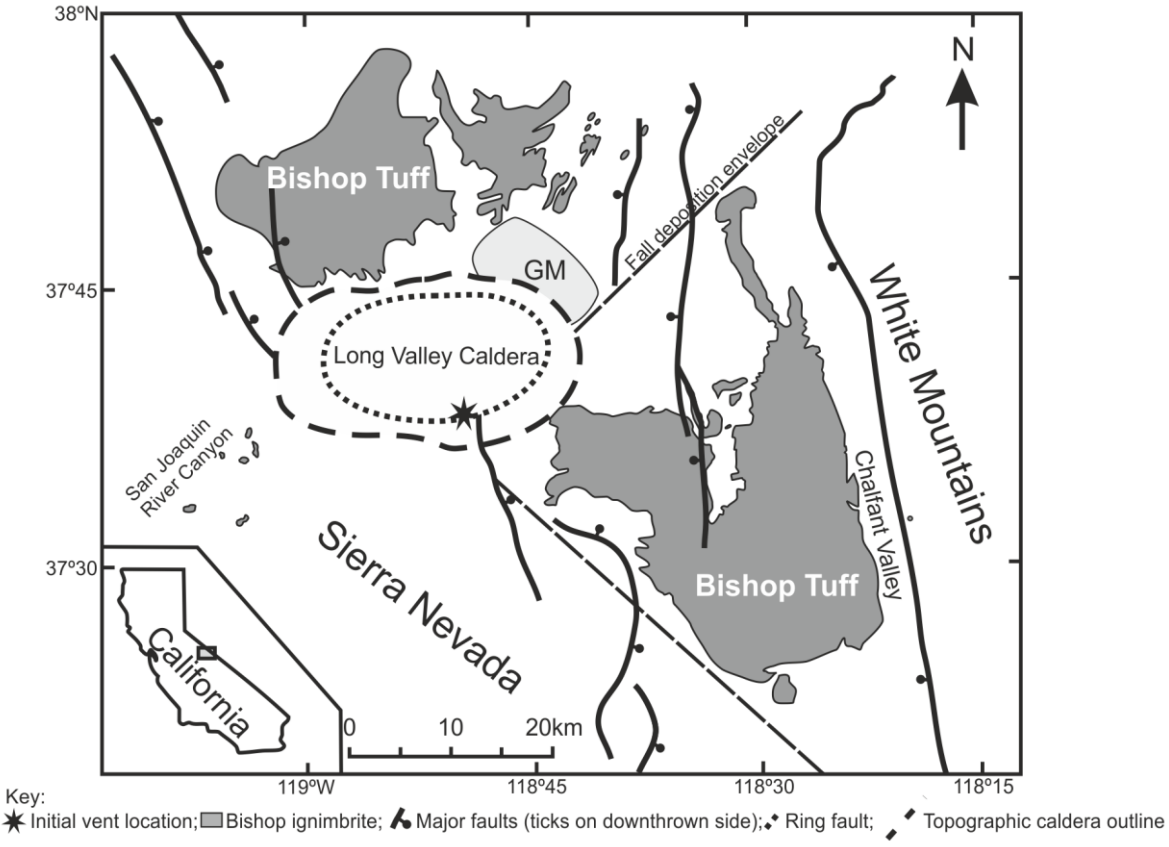

Fig. 1. Map of the Long Valley area, eastern California, USA, after Hildreth & Wilson (2007). The approximate initial vent location is after Hildreth & Mahood (1986). Regions of present-day outcrops of Bishop ignimbrite are highlighted in dark grey. The envelope enclosing precursory Glass Mountain (GM) lava domes is shown in light grey. The line marked 'Fall deposition envelope' marks the westerly limits of Bishop fall deposits found in the proximal area shown in this map.

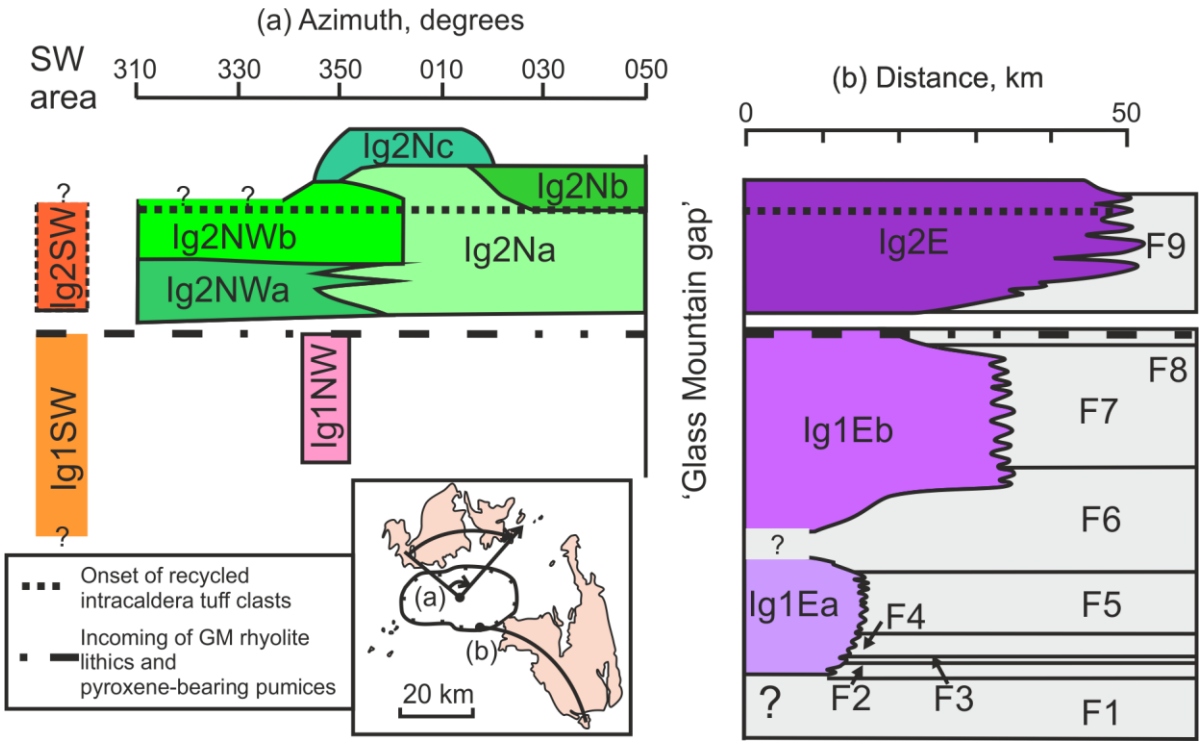

1473

1474 **Fig. 2.** Summary of the stratigraphy of the Bishop Tuff, after Hildreth & Wilson (2007).

1475 Ignimbrite units are coloured: purple for the early-erupted units; green for the late-

1476 erupted units, with subordinate units in orange and pink. Fall units are in grey. Panel

1477 (a) shows a hypothetical cross section from NW to NE through the northern

1478 ignimbrite lobes as viewed from the centre of Long Valley caldera. Panel (b) is a

1479 schematic proximal to distal cross-section approximately along the line of Owens

1480 River Gorge, where the horizontal axis represents distance from the initial vent site of

1481 Hildreth & Mahood (1986). GM refers to Glass Mountain.

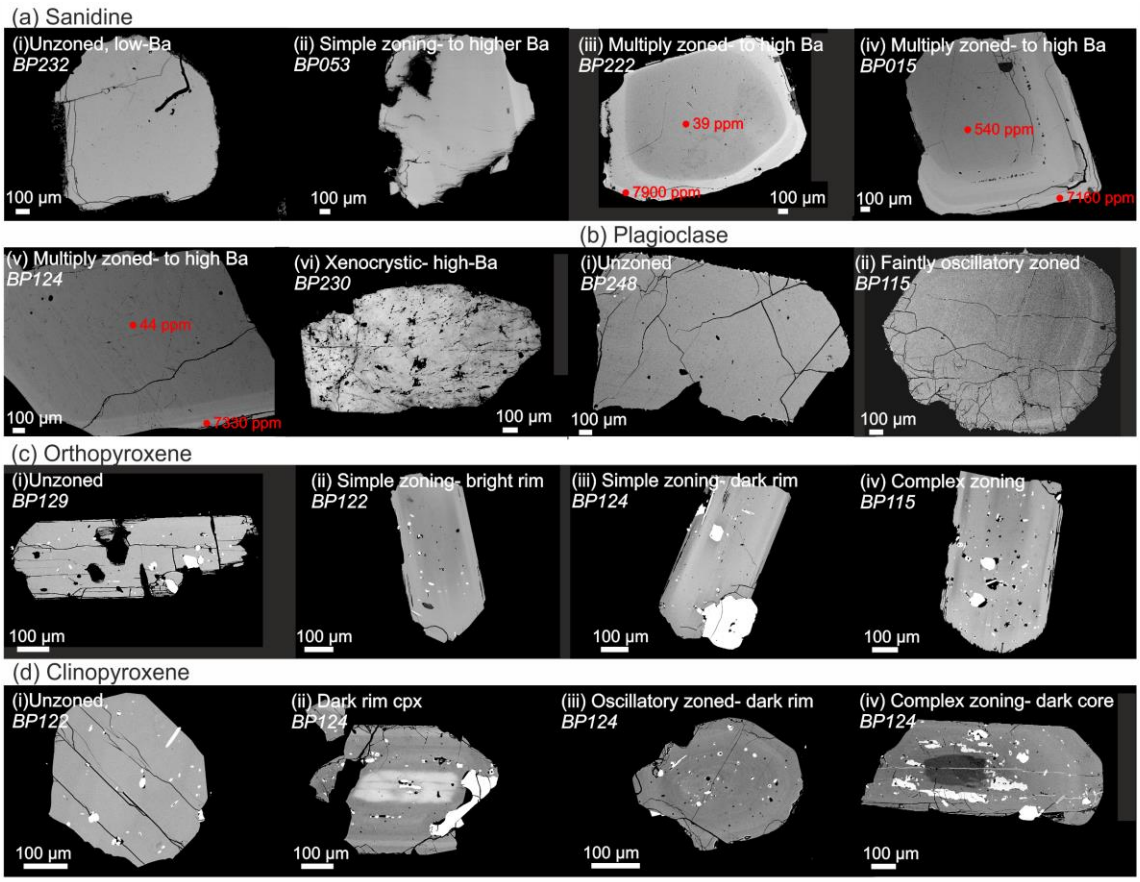

Fig. 3. Representative images to show the examples of textural variation observed in the common mineral phases found in Bishop pumices where sample numbers in italics relate to those in Table 1 (see Chamberlain *et al*., 2014a, for zircon zonation patterns). Panel (a) shows the different types of sanidine zoning identified from BSE imagery with Ba concentrations from cores and rims labelled in red, and panel (b) shows the normally unzoned plagioclase, and the subordinate oscillatory zoned plagioclase (BSE images). Panels (c) and (d) show the variations observed in BSE images of pyroxenes ranging from unzoned through to complexly zoned, where a brighter BSE shade in the rim represents higher Fe (and lower Mg) content, and a darker shade represents lower Fe (and higher Mg) content compared with the core. In all images the scale bar is 100 µm in length.

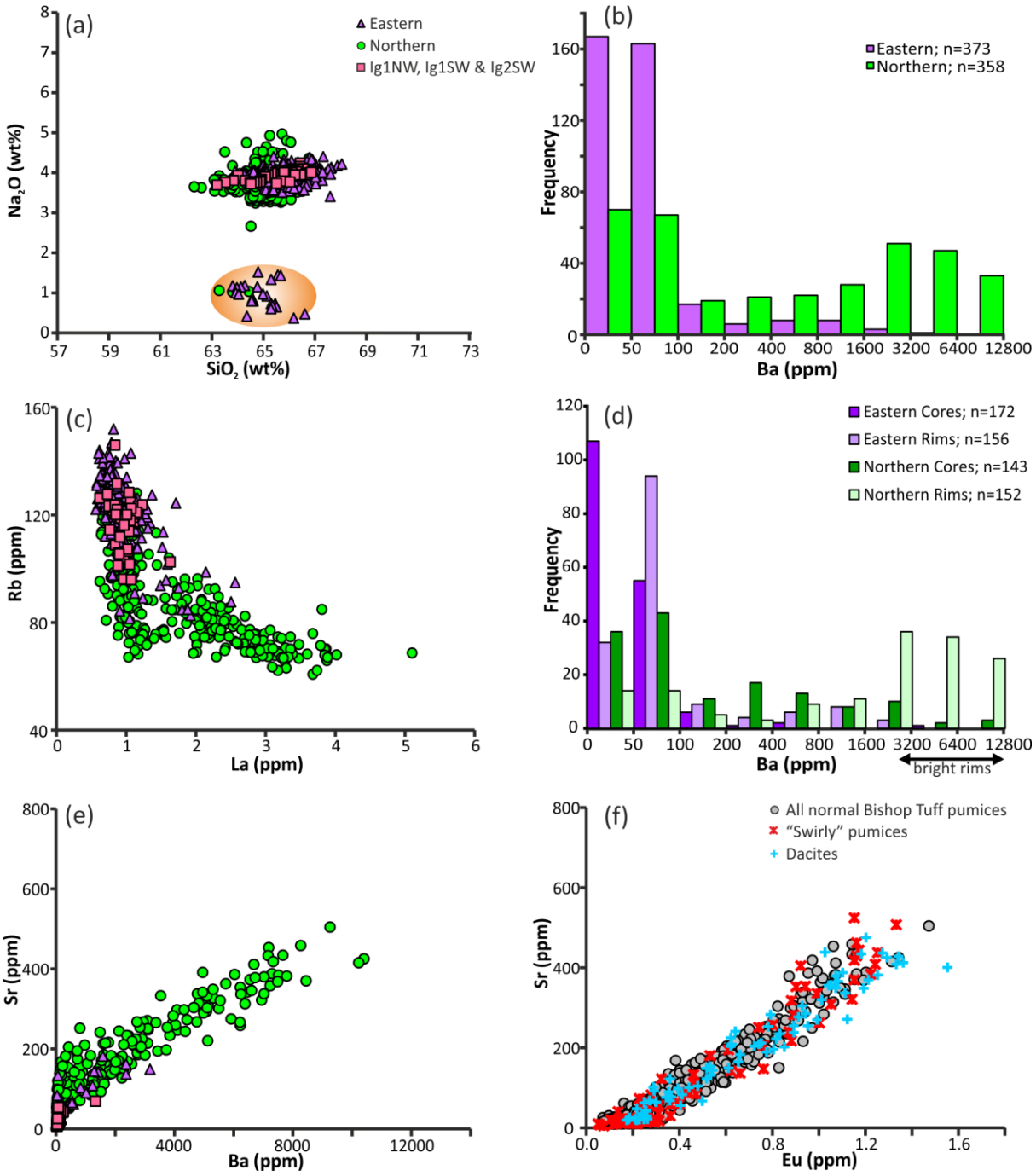

1494

1495 **Fig. 4.** Major (a) and trace (b to f) element variations in sanidines. Purple filled triangles
1496 represent sanidine analyses from 'normal' eastern samples; green filled circles
1497 'normal' northern samples and pink filled squares are analyses from pumices in
1498 Ig1NW, Ig1SW and Ig2SW. Xenocrystic sanidines are outlined in orange on panel (a)
1499 but are not shown in any trace element plots. (a) Major element variation in Bishop
1500 sanidine; (b) Histogram of Ba (ppm) for all analyses of sanidine from normal eastern-

and northern-sourced samples; (c, e) Trace element variation in Bishop sanidine; (d) Histogram of Ba (ppm) for sanidine cores (darker) and rims (lighter) from eastern- (purple) and northern-sourced (green) 'normal' Bishop samples; (f) comparison of all normal Bishop sanidine analyses (eastern- and northern-sourced) with sanidine from variant (swirly and dacitic) pumice types. The approximate range in 'bright rim' Ba concentrations are shown on (d) by the arrow. The full data sets (and uncertainties) are given in Electronic Appendices 1 and 2.

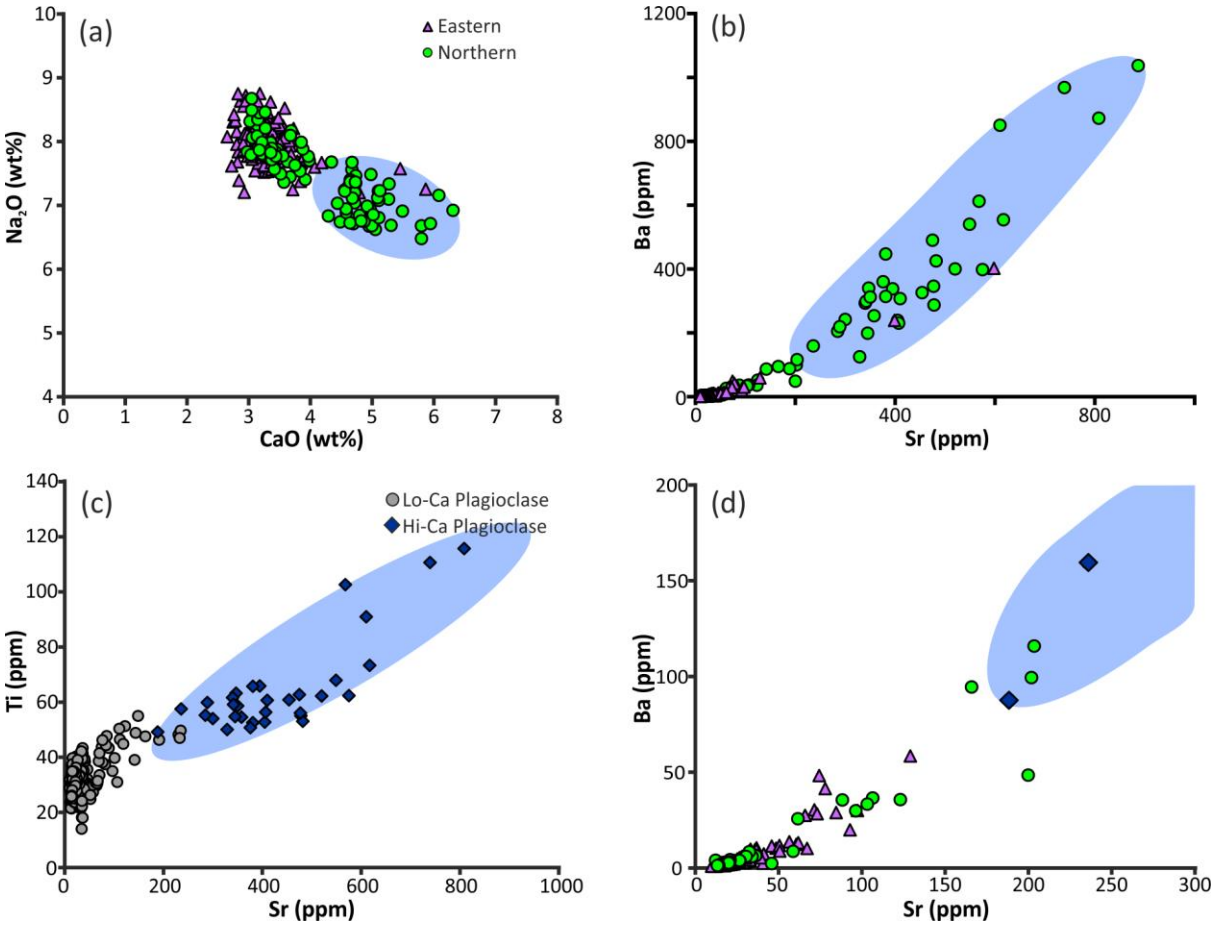

Fig. 5. Major (a) and trace (b, c, d) element variations in plagioclase from Bishop Tuff samples, where (d) is and enlargement of (b) to show the overlap in composition of lower-Ca plagioclase from both northern and eastern samples. Purple filled triangles represent eastern material; green filled circles northern material. The higher-Ca plagioclase group is outlined by the blue field. The full data sets (and uncertainties) are given in Electronic Appendices 1 and 2.

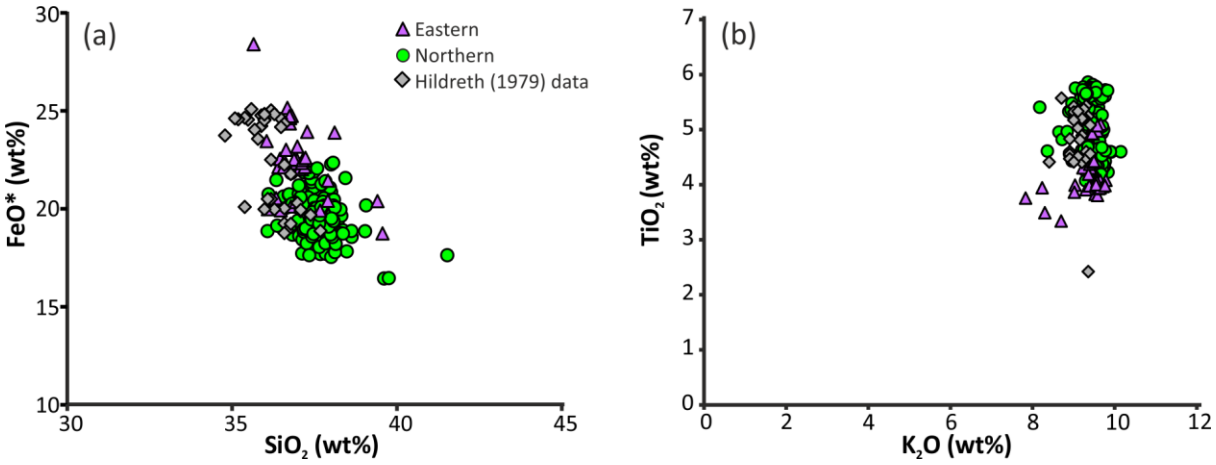

Fig. 6. Biotite major element variations from Bishop Tuff samples. Panels (a) and (b) highlight the influence of alteration within the Bishop samples, especially those from the eastern Bishop Tuff. For comparison, the data of Hildreth (1979) are plotted as grey diamonds. The full data sets (and uncertainties) are given in Electronic Appendices 1 and 2.

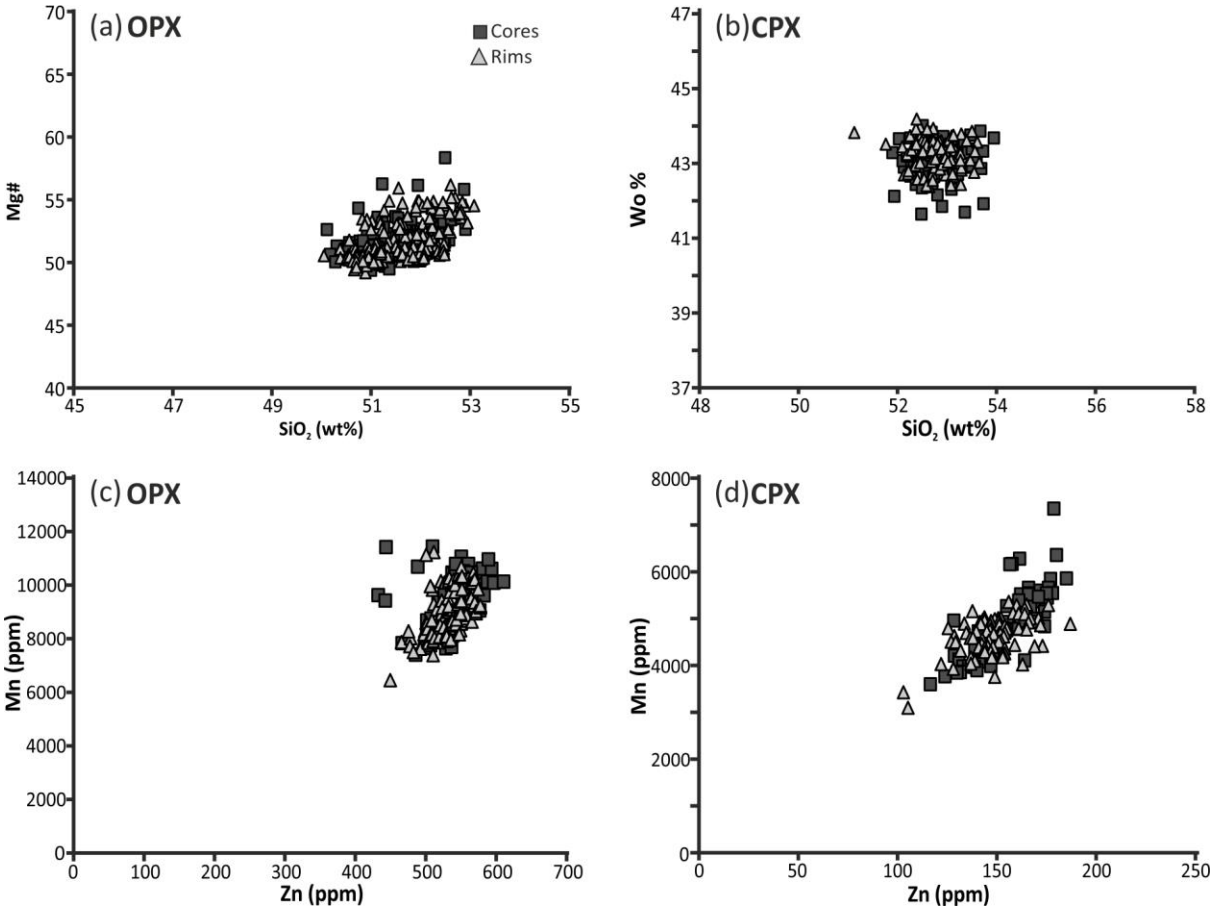

Fig. 7. Major (a, b) and trace (c, d) element compositions of pyroxenes from northern units of the Bishop Tuff. Orthopyroxene (OPX) analyses are presented in the left column (panels a, c); clinopyroxene (CPX) in the right column (panels b, d). Cores are plotted as filled squares, rims as filled triangles. The full data sets (and uncertainties) are given in Electronic Appendices 1 and 2.

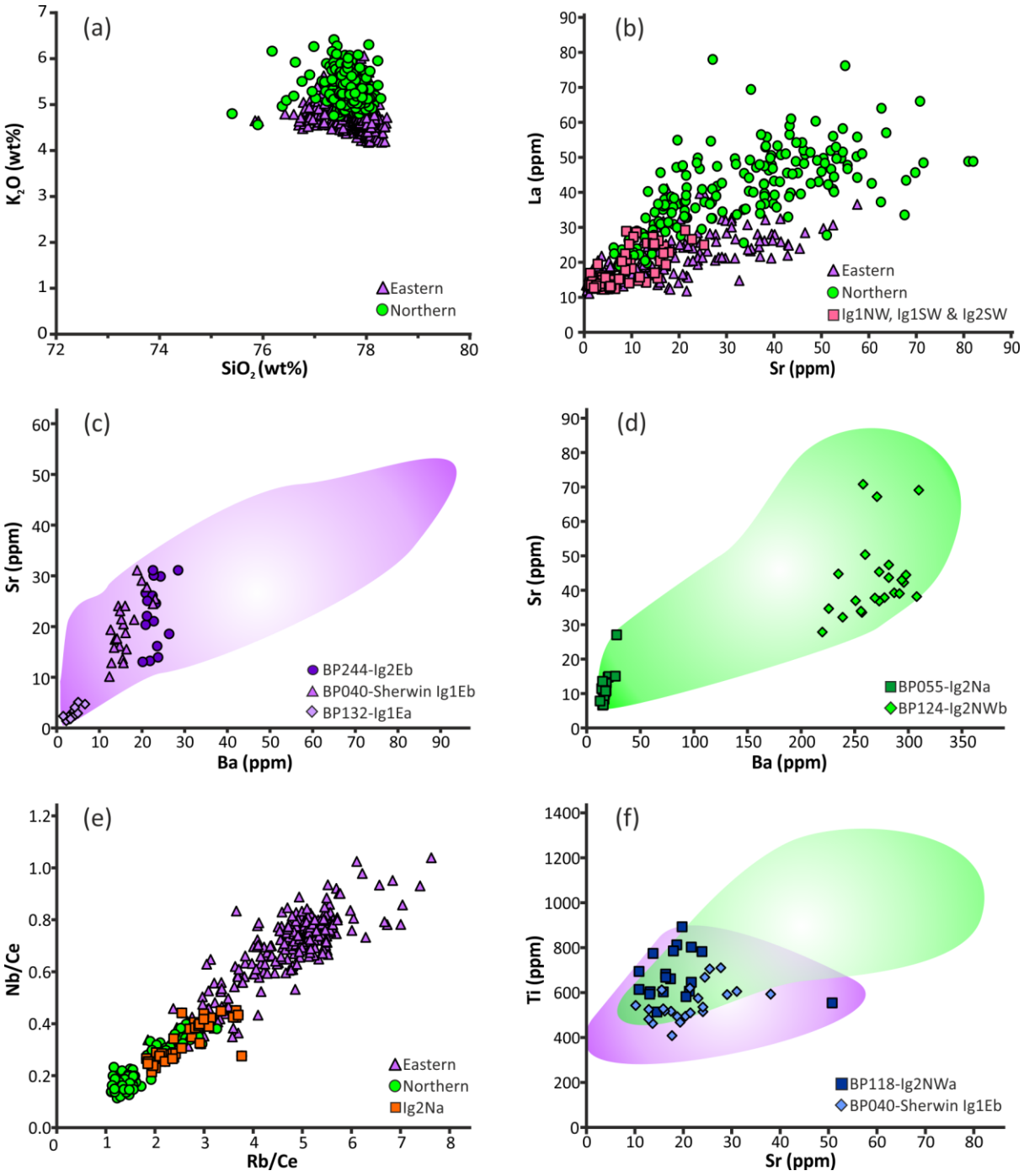

Fig. 8. Major (a) and trace (b to f) element variations in glass from samples in the crystal-poor to crystal-rich range of 'normal' pumices (as defined by Hildreth & Wilson, 2007) of the Bishop Tuff. Eastern samples are plotted as purple filled triangles (or purple fields); northern samples as green filled circles (or green fields). Ig1NW, Ig1SW and Ig2SW data are plotted as pink filled squares in panel (b); Ig2Na data as orange filled squares in panel (e). Illustrative representative single sample variations

1536 are shown in panels (c) and (d) – but note the contrast in scales – with the range in all
1537 eastern (purple) and northern (green) samples demonstrated by the fields plotted in
1538 (c), (d) and (f). The full data sets (and uncertainties) are given in Electronic
1539 Appendices 1 and 2.

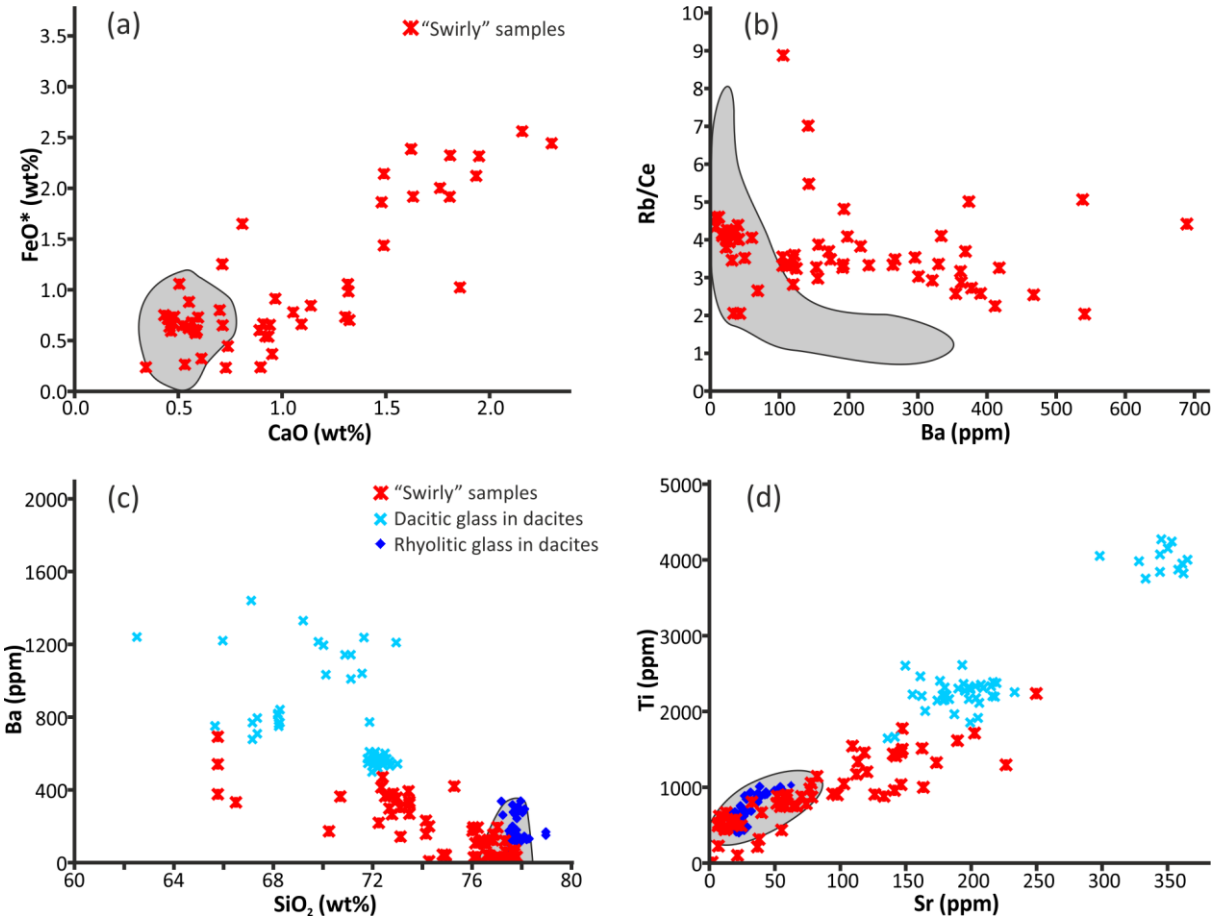

Fig. 9. Major (a) and trace (b to d) element variations in glass from samples in the range of 'variant' pumices (as defined by Hildreth & Wilson, 2007) in the Bishop Tuff compared with those measured from all 'normal' Bishop pumices (grey field): swirly pumices are red crosses, dacitic pumices are blue symbols, where lighter crosses are the dacitic glass in the dacite samples, and darker diamonds are the rhyolitic glass in the dacite samples. The dacite data plotted includes both the white admixed rhyolitic portions (as blue diamonds) and darker, dacitic portions (as blue crosses) of the dacite clasts. The full data sets (and uncertainties) are given in Electronic Appendices 1 and 2.

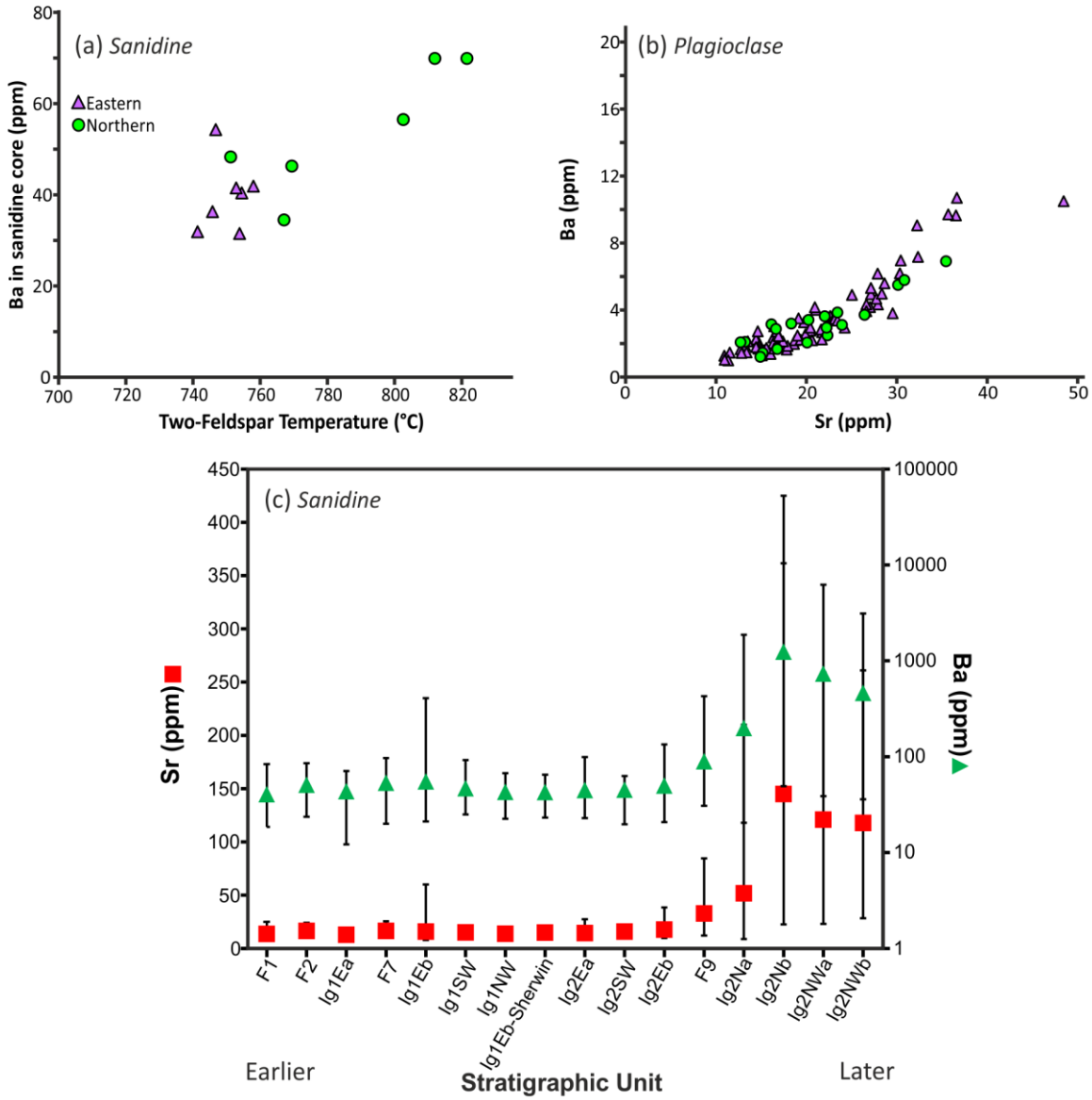

Fig. 10. Summary of crystal core compositional data providing evidence for thermal and compositional stratification within the Bishop Tuff prior to introduction of the 'bright-rim' magma. (a) Two-feldspar temperatures from Chamberlain *et al*. (2014b) plotted against the respective Ba content of sanidine cores from which the temperature was calculated. Eastern samples are purple filled triangles; northern samples are green filled circles. Panel (b) shows trace element variations in plagioclase cores: eastern samples are purple filled triangles; northern samples are green filled circles. Panel (c) shows the averages (as single points) and ranges (as bars) of trace element

concentrations in sanidine cores ordered by stratigraphic position and eruptive ordering, where green triangles refer to Ba data, and red squares refer to Sr data.

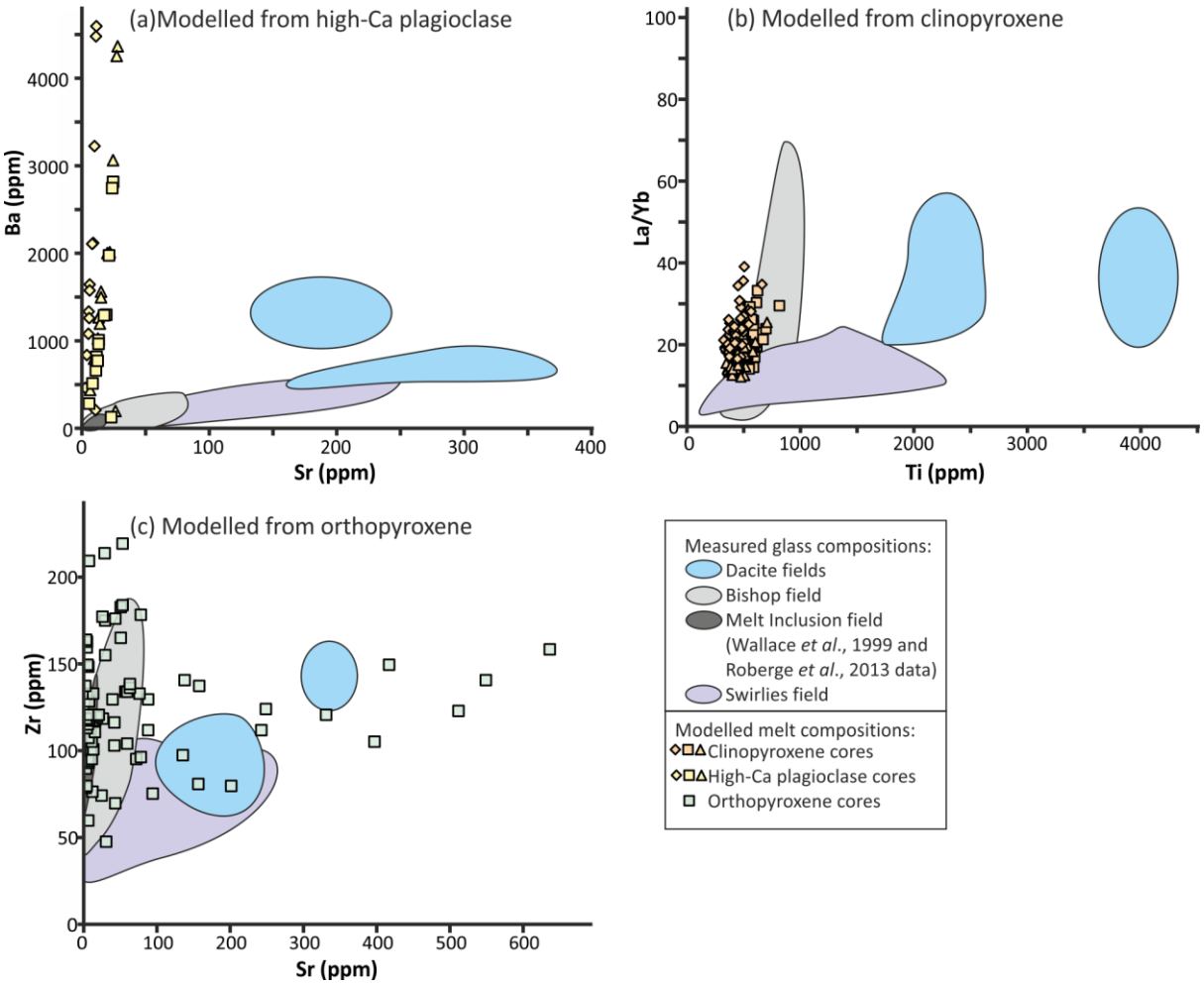

1561

1562 **Fig. 11.** Modelling of inferred melt compositions from (a) high-Ca plagioclase (b)

1563 clinopyroxene and (c) orthopyroxene. The field of all Bishop glass data is shown in

1564 light grey, the range in melt inclusion compositions from Roberge *et al*. (2013) in dark

1565 grey, and the field for glass compositions of variant swirly pumices in purple. Dacite

1566 glass fields are shown in blue. Modelled glass compositions from clinopyroxene cores

1567 are shown as orange points, using the partition coefficients of Olin & Wolff (2010).

1568 Modelled glass compositions from higher-Ca plagioclase cores (yellow points) and

1569 from orthopyroxene cores (green points) are calculated from the multiple partition

1570 coefficients given by Brophy *et al*. (2011). Different shaped symbols in panels (a) and

1571 (b) indicate modelled melt compositions from the various partition coefficients

1572 calculated with each respective study.

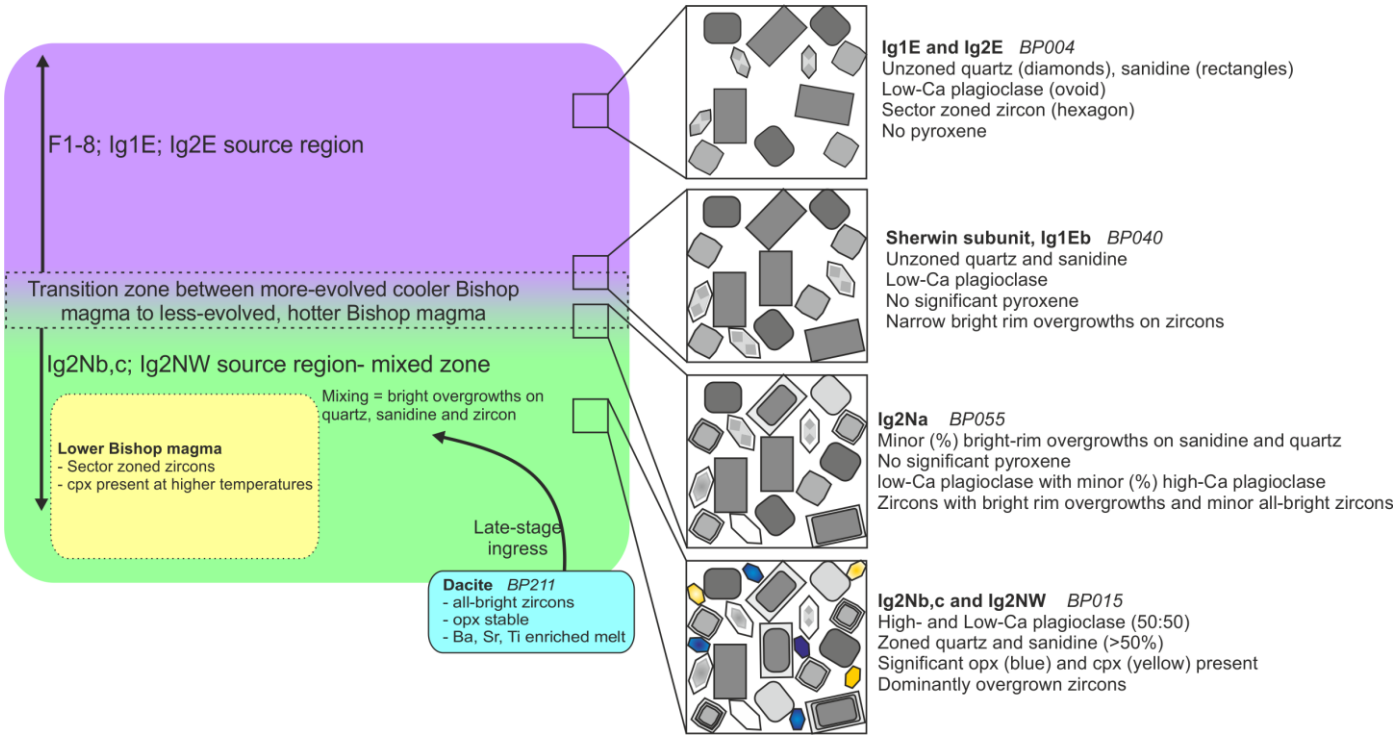

Fig. 12. Cartoon of the Bishop magma chamber showing the inferred origins for the crystal species (including those native to the late-stage incoming 'bright-rim' magma or dacites) and their compositional variations found in different eruptive units of the Bishop Tuff. Examples of eruptive units (from Hildreth & Wilson, 2007) are detailed in bold, with specific representative sample numbers from this study (listed in Table 1) in italics. Variant pumice types are not shown for simplicity. See text for discussion.

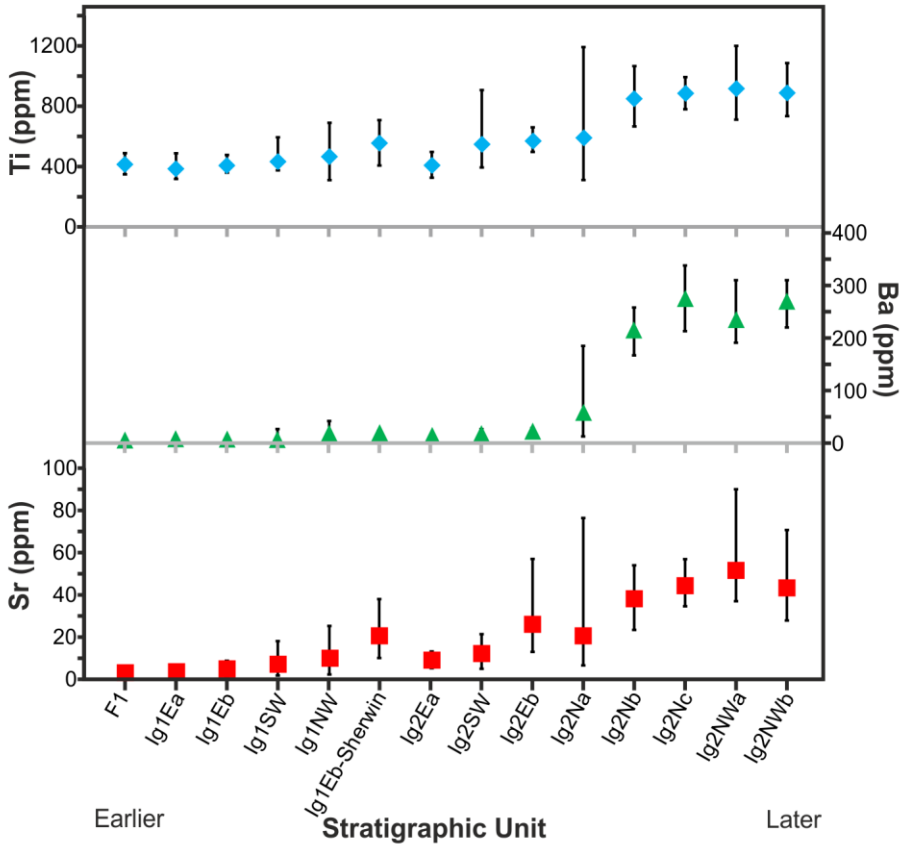

1581

1582

1583 **Fig. 13.** Plot of mean values and total ranges of variation in key trace element concentrations

1584 in glass of the Bishop Tuff ordered by stratigraphic unit and eruptive ordering.

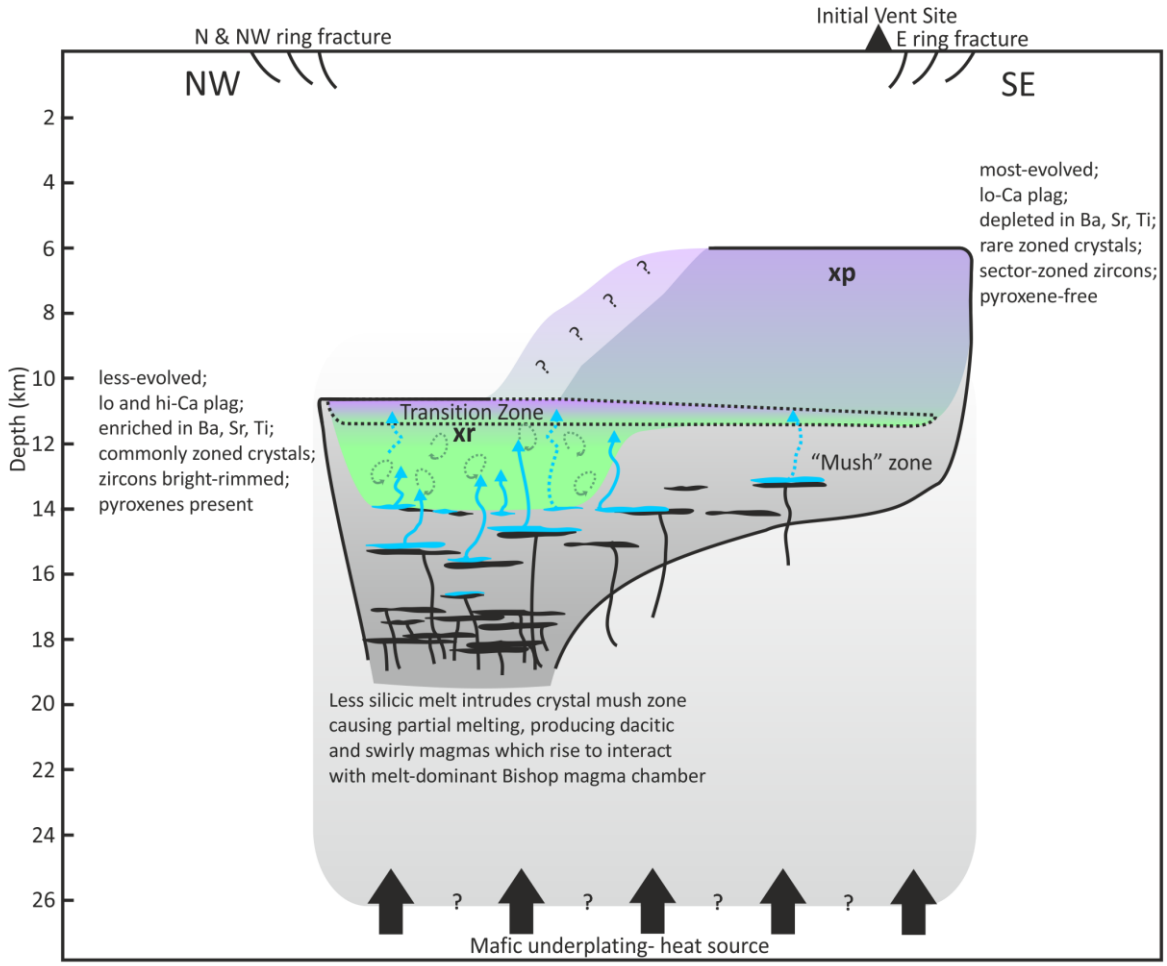

1585

1586 **Fig. 14.** A revised model for the immediately pre-eruptive Bishop magma chamber derived
1587 from this work and utilising the depth estimates of Wallace *et al*. (1999). Black sills
1588 and dykes represent less-evolved compositions than the blue sills and dykes which
1589 represent the 'bright rim' magma. See text and Fig. 12 for discussion of various
1590 crystal origins.

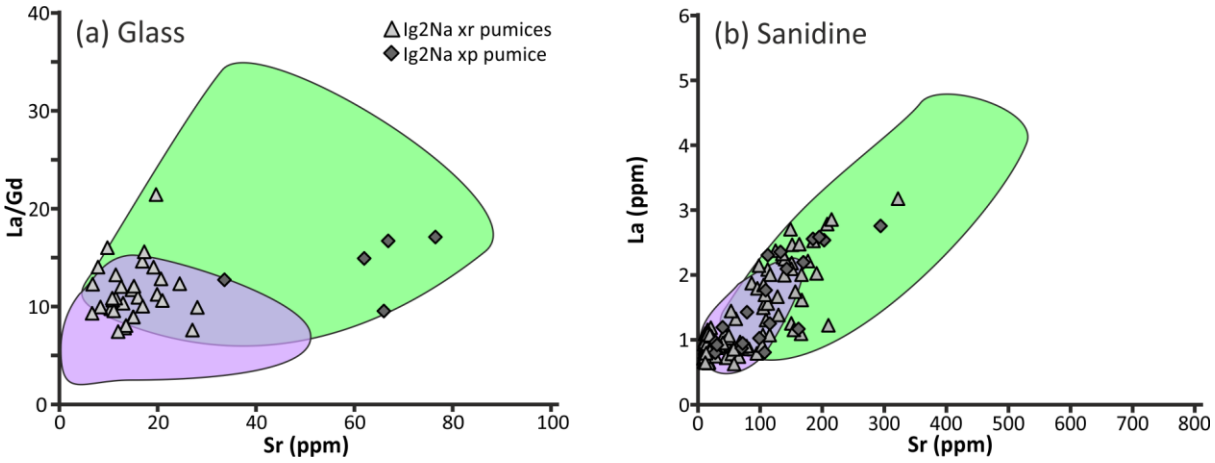

Fig. 15. Comparison of crystal-poor (xp) and crystal-rich (xr) samples from package Ig2Na, showing (a) glass and (b) sanidine trace element concentrations compared with the ranges of concentrations from all eastern (purple shaded area) and northern (green shaded area) samples. Analyses from the xp sample (purple filled diamonds) of Ig2Na should overlap with the purple eastern field if it represented 'eastern-type' magma that was present in the part of the chamber tapped by the northern vents. Analyses from crystal rich samples are plotted as green triangles. The full data sets (and uncertainties) are given in Electronic Appendices 1 and 2.